TECHNISCHE UNIVERSITÄT WIEN

Doctoral Thesis

Effect of polyquaternary ammonium polymer on the electrochemical deposition of zinc

zur Erlangung des akademischen Grades

Doktor der technischen Naturwissenschaften

an der Fakultät für

Technische Physik

eingereicht von

MSc. Gastelle F. Tiétcha
Matrikelnummer 11743116

ausgeführt am Institut für Angewandte Physik
der Fakultät für Physik der Technischen Universität Wien

Betreuer: Univ.Prof. Dipl.-Ing. Dr.techn. Markus Valtiner
Mitbetreuer: Dr. Laura L. E. Mears

_____ _____ _____
Ort, Datum   (Unterschrift Verfasser)   (Unterschrift
Betreuer)

2

Ich erkläre an Eides statt, dass ich die vorliegende Dissertation selbstständig und ohne fremde Hilfe unter der Betreuung von Univ. Prof. Dipl.-Ing. Dr.techn. Markus Valtiner verfasst habe. Es wurden keine anderen als die angegebenen Quellen und Hilfsmittel benutzt bzw. die wörtlich oder sinngemäß entnommenen Stellen als solche kenntlich gemacht.

Herdecke, am 31.10.2023

À mon arrière-grand-mère, maman Clotilde Tchamdjié, qui malgré l'époque et l'environnement dans lesquels elle a vécu, croyait en l'éducation de la femme et en son impact dans la société. Je n'ai plus aucun souvenir d'elle, mais je sais néanmoins que c'est grâce à elle si j'ai pu écrire cette thèse doctorale. J'ai appris que l'un de ses plus grands rêves de jeunesse avait été d'apprendre à écrire, ne serait-ce que son nom. Elle n'a pas pu réaliser se rêve de son vivant, mais le fait aujourd'hui à travers moi par cet hommage que je lui rends. Que son âme repose en paix.

Acknowledgments

This adventure began a few years ago when I was writing my master's thesis at the company Dörken Coatings GmbH. The research work for my master's thesis was drawing to a close when my laboratory supervisor, Dr. Ingo Klüppel, asked me a surprising question. I can remember the exact day when he asked, "Can you imagine starting a doctoral thesis with us?" The idea excited me, but at the same time it scared me a little. Because I wasn't sure whether I would have the strength to carry the project through to its end. I would therefore like to thank Ingo very much for the chance he gave me back then. He supported me during the last years and gave me professional and moral assistance. I have learnt a lot from him. I would also like to take this opportunity to thank Dr. Laura Mears from the depth of my heart. Words alone would not be enough to express my gratitude. I could not have imagined a better tutor for my dissertation. Thanks to her excellent professional and friendly support, I was able to easily overcome all the frustrations and challenges that a PhD student can go through during their dissertation. I am so happy that I was able to get to know Laura and hope that we will keep in touch. I would like to thank Prof. Dr. Markus Valtiner for accepting to supervise this project a few years ago. I could not have imagined a better supervisor. I would also like to take this opportunity to thank the company Dörken Coatings GmbH, especially the head of the department for research and development, Dr. Marcel Roth, for allowing me to start in the company as a Master's student many years ago. I would then like to thank all the other members of Prof. Dr. Markus Valtiner's working group for their help and willingness. Thanks to them, I felt like a princess during my pregnancy in Vienna. They looked after me and made sure that I didn't miss anything. They made my time in Vienna unforgettable. To all my colleagues at Dörken, I say thank you. Thank you for accepting me into the group from day one. Thank you for the friendly cooperation and for your friendship. I have only good memories of our cooperation.

Abstract

The market for zinc electroplating and demand for zinc coatings is increasing every year. This is because this process is the most cost effective for achieving reliable corrosion protection for a wide range of applications. Only when the protective zinc layer has almost completely dissolved (white rust formation), the base metal is attacked with the formation of red rust.

In this work we will use an alkaline cyanide-free galvanising process, the fastest growing segment of the industry, as it offers the possibility of being environmentally friendly. The cyanide-free zinc electrolyte consists of different inorganic and organic components, including polymers, which serve to inhibit the deposition reaction to enable the formation of smooth, shiny thin layers. Here, the effect of polyquaternium 2 on the mechanism of deposition and the structure of the deposited layer is closely observed. Understanding exactly how this system works can inform production of a material that offers a better film thickness distribution than conventional commercially available materials. We applied cyclic voltammetry (CV), X-ray photoelectron spectroscopy and quartz crystal microbalnce with dissipation to examine the kinetics of electrochemical zinc deposition moderated with polyquaternium 2. Subsequently, atomic force microscopy (AFM) and low energy ion scattering measurements were performed to see the influence of the polymer used in the structure of the deposited layer.

These techniques have demonstrated that the positively charged polymer interacts with the negatively charged zincate to form a polymer-zincate aggregate and this way facilitates the transport of the zincate to the negatively charged metal surface. Clear peak characteristics could be seen in cyclic voltammograms, indicating diffusion-controlled deposition of additional zinc ions. This is due to the polyquaternium 2 adsorbing on the metal surface after it has allowed the formation of the very first zinc layers. The polymer film is a physical, diffusion barrier to further zinc ions, thus allowing them time to find a suitable deposition site and preventing dendrite formation.

This statement is confirmed with AFM. The surface of the polymer free deposited layer shows crystals of different sizes with an uneven surface distribution. In the polymer moderated deposition, the layer shows longitudinal crystals of equal size with uniform surface distri-

bution. In the absence of polymer, we have a growth mechanism of the Volmer-Weber type (island growth mechanism), while in the presence of polyquaternium 2, the Stranski-Krastanov growth (layer-by-layer followed by an island growth) dominates.

The deposition is also related to the molar mass and chain flexibility of the polymer. By replacing the crosslinker, we were able to bring more flexibility to the backbone and thus produce a polymer that inhibits more strongly in higher current density regions. We were also able to develop a method in the course of this work that allows monitoring of the deposited layer in real time. There is a lot of potential in this method, as it can be used for real-time quality control of the electrolyte in the electroplating industry in the future.

Kurzfassung

Der Markt für die galvanische Verzinkung und die Nachfrage nach Zinküberzügen nimmt jedes Jahr zu. Das liegt daran, dass dieses Verfahren das kostengünstigste ist, um einen zuverlässigen Korrosionsschutz für eine Vielzahl von Anwendungen zu erreichen. Erst wenn sich die schützende Zinkschicht fast vollständig aufgelöst hat (Weißrostbildung), wird das Grundmetall unter Bildung von Rotrost angegriffen.

In dieser Arbeit wird ein alkalisch-cyanidfreies Verzinkungsverfahren verwendet, das am schnellsten wachsende Segment der Industrie ist, da es die Möglichkeit bietet, umweltfreundlich zu sein. Der cyanidfreie Zinkelektrolyt besteht aus verschiedenen anorganischen und organischen Komponenten, darunter auch Polymere, die dazu dienen, die Abscheidungsreaktion zu hemmen, um die Bildung glatter, glänzender dünner Schichten zu ermöglichen. Hier wird die Wirkung von Polyquaternium 2 auf den Abscheidungsmechanismus und die Struktur der abgeschiedenen Schicht genau beobachtet. Wenn man genau versteht, wie dieses System funktioniert, kann man ein Polymer herstellen, das eine bessere Schichtdickenverteilung aufweist als herkömmliche, im Handel erhältliche Stoffe. Wir haben zyklische Voltammetrie (CV), Röntgenphotoelektronenspektroskopie und Quarzkristallmikrowaage mit Dissipation angewandt, um die Kinetik der elektrochemischen Zinkabscheidung zu untersuchen, die mit Polyquaternium 2 moderiert wird. Anschließend wurden Rasterkraftmikroskopie (AFM) und Niederenergetische Ionenstreuspektroskopie Messungen durchgeführt, um den Einfluss des verwendeten Polymers auf die Struktur der abgeschiedenen Schicht zu ermitteln.

Diese Techniken haben gezeigt, dass das positiv geladene Polymer mit dem negativ geladenen Zinkat interagiert, um ein Polymer-Zinkat-Aggregat zu bilden und auf diese Weise den Transport des Zinkats zur negativ geladenen Metalloberfläche zu erleichtern. In den CVs waren deutliche Peak-Charakteristika zu erkennen, die auf eine diffusionsgesteuerte Ablagerung zusätzlicher Zinkionen hinweisen. Dies ist darauf zurückzuführen, dass das Polyquaternium 2 an der Metalloberfläche adsorbiert, nachdem es die Bildung der allerersten Zinkschichten ermöglicht hat. Der Polymerfilm stellt eine physikalische Diffusionsbarriere für weitere Zinkionen dar, so dass diese Zeit haben, einen geeigneten Ablagerungsort zu finden, und dadurch eine

Dendritenbildung verhindert wird.

Diese Aussage wird mit AFM bestätigt. Die Oberfläche der polymerfreien Ablagerungsschicht zeigt Kristalle unterschiedlicher Größe mit einer ungleichmäßigen Oberflächenverteilung. Bei der polymermoderierten Abscheidung weist die Schicht längliche Kristalle gleicher Größe mit gleichmäßiger Oberflächenverteilung auf. In Abwesenheit des Polymers haben wir einen Wachstumsmechanismus vom Volmer-Weber-Typ (Inselwachstum), während in Anwesenheit von Polyquaternium 2 das Stranski-Krastanov-Wachstum (Layer-by-layer, gefolgt von einem Inselwachstum) dominiert.

Die Abscheidung hängt auch mit der molaren Masse und der Kettenflexibilität des Polymers zusammen. Durch den Austausch des Vernetzers konnten wir mehr Flexibilität in das Rückgrat bringen und so ein Polymer herstellen, das in Bereichen mit höherer Stromdichte stärker hemmt. Außerdem konnten wir im Rahmen dieser Arbeit eine Methode entwickeln, die eine Überwachung der abgeschiedenen Schicht in Echtzeit ermöglicht. In dieser Methode steckt viel Potenzial, da sie in Zukunft zur Echtzeit-Qualitätskontrolle des Elektrolyten in der Galvanikindustrie eingesetzt werden kann.

Contents

Contents

x

Glossary

Abbreviations	Meaning
AFM	Atomic Force Microscopy
CV	Cyclic Voltametry
EDL	electric double layer
GPC	Gel permeation chromatography
HER	Hydrogen Evolution Reaction
HS-LEIS	High Sensitivity-Low Energy Ion Scattering
LEIS	Low Energy Ion Scattering
OCP	Open Circuit Potential
PQ	Polyquaternium 2
PEEK	Polyether Ether Ketone
QCM-D	Quartz Crystal Microbalance with Dissipation
RMS	Root Mean Square
XPS	X-ray Photoelectron spectroscopy

Contents

Symbols	Meaning
Γ	Surface density
R_F	Flory Radius
η_s	Number of Segments
l_s	Length of a Segment
ν	Flory constant
R_g	Radius of gyration
D	Distance between chains
X_n	Degree of polymerization
p	Conversion
r	Ratio of number of functional group
N_A	Number of functional group A
N_B	Number of functional group B
M_W	Average molecular weight of polymer
M	Molecular weight of the repeating unit
z	Number of transferred electrons
F	Faraday constant
T	Temperature
R	Gas constant
E_{Me}^0	Standard electrode potential of the mentioned species
c_i	Concentration of the mentioned species
f_i	Activity coefficient of the mentioned species
a_i	Activity of the mentioned electroactive species
η	Overvoltage
E	Electrode potential
$E_{Me/Me^{z+}}$	Equilibrium electrode potential
U	Measured voltage
I	Current through the conductor
R	Resistance of the conductor
i_0	Exchange current density
α	Penetration factor
Q	Electric charge
n	Number of moles
t	Time
m	Mass
H	Enthalpy
S	Entropy
G	Gibbs free energy

1 Industrial question and motivation

Surface treatments are nowadays integrated into almost all technical products. This means that surface technology can be seen as a cross-sectional technology. Mostly, materials such as unalloyed steel or grey cast iron are used for various parts in industry for cost reasons. However, these are not very resistant to environmental influences and would show the first signs of corrosion after a short time. If a component corrodes, not only does its appearance deteriorate, but also its functional properties. The modification of surfaces can lead to an improvement of the technical and functional properties of parts. Thanks to these treatments, for example, optical properties, corrosion and wear resistance are improved. Surface modification can not only be used for decorative purposes, but can also change the electrical properties of a component. It is therefore used in different sectors such as the automotive industry, the jewellery industry, the mechanical engineering sector, the IT sector, etc. to name only a few. It is definitely cheaper to coat steel with a noble metal layer than to use an expensive noble metal directly.

There are different methods to treat surfaces, among others galvanising. Nickel plating, zinc plating, silver plating are a few galvanic processes used in industry to produce metallic coatings. Of all these methods, zinc plating is the cheapest and this would explain why it is so widely used. Parts can be zinc electroplated by three different processes: acidic, alkaline cyanide and alkaline cyanide free galvanising (Chapter 2.6). The layers that result from the three electrolytes are equivalent in terms of corrosion protection. Which electrolyte is used therefore depends on the following criteria:

- Type of base material

- Degree of contamination of the base material

1

- Shape of the parts

- Purpose of the layer

- Problems with waste water.

Taking into account the limitations mentioned above, the choice of electrolyte can only be based on economic efficiency. The economy depends on the deposition rate, energy costs, chemical and metal consumption etc... A short comparison between alkaline and acid zinc processes can be found in the table 1.1.

Table 1.1: Comparison between the acidic and the alkaline zinc electroplating baths.

Acidic	Alkaline
pH: 3.5 - 5.5	pH $\geq$ 12
Zn^{2+} available in the electrolyte	Zincate complex available
Deposition is fast (1.5 μm/min)	Deposition is slow (0.5 - 1 μm/min)
Coarse grained	Fine grained
Inhomogeneous thickness distribution	More homogeneous thickness distribution

Nowadays, demands on the processes are always increasing. They should be as cheap as possible, allow the formation of good-looking and target-fulfilling layers and finally avoid the use of toxins. The latter is the reason why research in the field of alkaline cyanide free electrolytes is getting stronger and stronger. As the cyanide based baths are toxic due to their composition.

It is more than a century since Snowdon investigated the properties that influence the electrolytic deposition of zinc.[1] He found that deposition from an alkaline zinc bath is smoother than from an acidic one. He also made one of the first investigations on the use of organic additives (resorcinol) in the zinc bath [1]. Subsequently, electroplating of zinc has become very important for the metal industry. In particular the complexity of the baths has increased, with a lot of research on the additives that positively influence zinc deposition.[2–7] The purpose of using those additives is firstly in order to achieve a better working efficiency of the electrolyte, through improvement of the current efficiency or the anodic depolarisation. The second purpose is to achieve a better physical appearance and properties of the deposited layer through

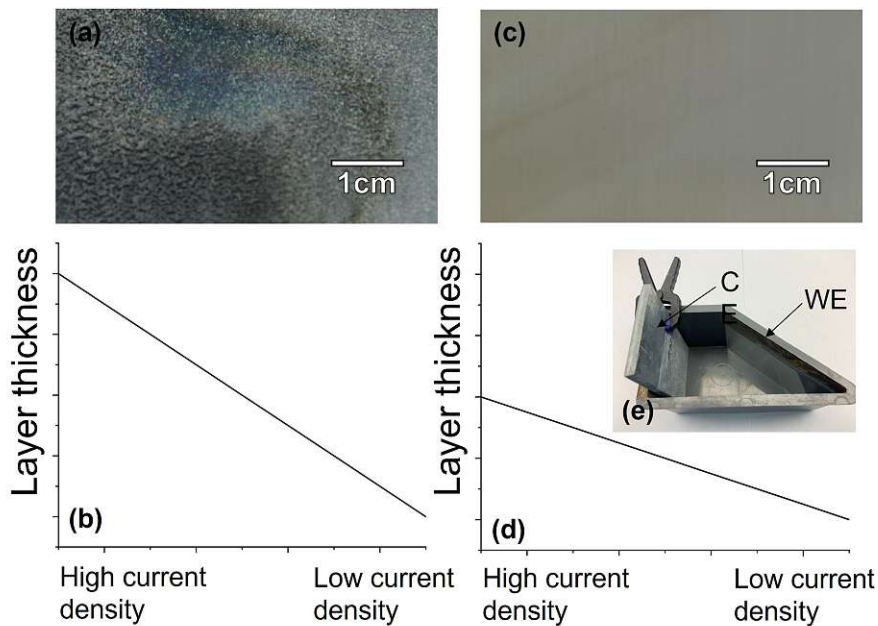improvement of the grain size and the brightness. Figure 1.1 shows

Figure 1.1: Photography of a sheet and their layer thickness distribution showing: (a) a Zinc layer deposited without PQ, (c) a Zinc layer deposited with PQ and (b) and (d) the corresponding layer thickness distributions. (e) Picture of a Hull-cell with the cathode and the anode represented.

the influence of an additive particularly clearly with the images of two different zinc layers deposited on a steel sheet. In Figure 1.1(a) the zinc layer was deposited from an alkaline zinc bath containing no polymer additive. The deposited layer is matte, rough and has an uneven layer distribution. On the high current density side the deposited layer appears as a fine powder-like structure. In addition, the coating does not adhere well to the steel part. In Figure 1.1 (c) polyquaternium 2 polymer (PQ) was included as an additive. With this additive the deposited layer appears smooth, bright and has a more even layer distribution. The dramatic differences in the colour and homogeneity of the coating are not the only parameters that the additive influences. As is shown further in Figures 1.1(b) and (d) the layer thickness distribution of the zinc on the steel sheet is also changed by the additive. For both sets of conditions from the left to the right side of the sheet, the layer thickness decreases, which arises from the current density gradient created during deposition in a Hull-cell (see Figure 1.1 (e)). A Hull-cell [8] is a laboratory scale version of a standardised electroplating system. It consists of a trapezoidal container made of an insulator. The elec-

trodes are arranged in such a way that cathodic or anodic effects can be observed over wide current density ranges. Bath parameters, such as additive concentrations, pH, temperature, electrolyte composition etc. influence the properties of the deposited layer. The hull cell is designed to determine these influences as a function of the current density by varying the distance between the steel cathode and the steel anode. Figure 1.1 (d) shows that there is a greater reduction in thickness on the high current density side. This shows that PQ decreases the gradient of the slope of the distribution, which improves the layer thickness. However, the ideal case would be to have a constant layer thickness distribution over the whole sheet.

The real motivation of this work is to able to achieve the ideal case or to realise results that are closer to the ideal case of the layer thickness distribution. So for this purpose, the following questions are open:

- What really happens at the interface during the polymer moderated deposition?

- Which crystallisation mechanism is followed during deposition?

- How does the polymer moderate the electrodeposition of zinc?

- What kind of polymer can inhibit the reaction in the high current density side and accelerates it in the low current density side?

- Is it possible to synthesise a polymer that will specifically influence the low or the high current density sides?

In the course of this work we will deal with the above questions.

2 Introduction

2.1 Electrochemistry and potential measurement

Electrochemistry [9, 10] deals with the relation between electrical and chemical processes. Either the redox reaction is forced by an externally applied electrical voltage (electrolysis), or a measurable voltage is caused by the chemical reaction of suitable substances (galvanic element). If a metal is immersed in a solution of its metal ions, an exchange reaction takes place at the phase boundary, which is dependent on the chemical potential of the individual contacting phases. The exchange reaction continues until the equilibrium potential is reached. The equilibrium potential is reached when the system is in equilibrium. How quickly equilibrium is reached depends on the exchange current density of the considered electrode reaction. Depending on which electrode is considered, either a reduction or an oxidation takes place. This corresponds to metal deposition for the reduction and metal dissolution for the oxidation. This reaction can generally be described by equation 2.1.

$$\text{Me}^{z+} + z e^- \rightleftharpoons \text{Me} \tag{2.1}$$
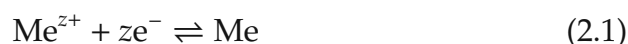
The potential of the electrode cannot be measured directly here, but only against a reference electrode. Usually, the reference electrode is the standard hydrogen electrode, whose electrode potential is set to zero by definition. For this work, however, Ag/AgCl electrode was used as the reference electrode. Thus, one measures a potential difference between an electrode and a reference electrode under standard conditions. In this way, one finally obtains the standard electrode potential of the individual redox pairs, which is summarised in the table of the electrochemical voltage series. With the help of the Nernst equation 2.2 , one can calculate the actual electrode potential in equilibrium. This equation gives the relationship between the potential of an electrode

and the activity of the ions involved in the electrode reaction.

$$E_{\text{Me/Me}^{z+}} = E^0_{\text{Me}} + \frac{RT}{z\text{F}} \ln \frac{a_{\text{Me}^{z+}}}{a_{\text{Me}}} \qquad (2.2)$$

With

$$a_i = f_i \cdot c_i \qquad (2.3)$$

a_i = activity of the mentioned electroactive species at the electrode interface

f_i = activity coefficient of the mentioned species

c_i = concentration of the mentioned species

E^0_{Me} = Standard electrode potential of the mentioned species

R = Gas constant (R = kN_A = 8.314 $\text{Jmol}^{-1}\text{K}^{-1}$)

T = Temperature in Kelvin

z = number of transferred electrons

F = Faraday constant (F = eN_A = 9.648·10^4 Cmol^{-1})

By applying an external voltage source to the electrodes, the equilibrium can be shifted in a desired direction. The deviation of the electrode potential, E, from the equilibrium potential $E_{\text{Me/Me}^{z+}}$ is called overpotential η, which is described by equation 2.4. Metal deposition happens when the equilibrium is shifted towards the metal.

$$\eta = E - E_{\text{Me/Me}^{z+}} \qquad (2.4)$$

The electrochemical investigations for this work were carried out with the help of a three-electrode system [9, 11]. For this purpose, a working electrode made of gold is used, on the surface of which the reaction of interest takes place. For the three-electrode arrangement, one also needs a reference electrode, which serves as the potential zero point, since its potential is constant. A setpoint voltage U_0 is applied between the working electrode and the non-polarisable reference electrode using a function generator. As soon as an electrochemical reaction takes place at the working electrode, the voltage U_{is} between the working and reference electrode changes according to Ohm's law:

$$U = R \cdot I \qquad (2.5)$$

A current is then sent from the counter electrode to the working electrode to bring the voltage back to the desired potential. To avoid measurement errors, no current should flow at the reference electrode, since its potential would be changed by this. The reference electrode was an Ag/AgCl electrode, while the counter electrode was made of platinum wire.

2.2 Electric double layer

When studying electrochemical reactions, the processes at the electrode/electrolyte interface are very important. When an electrode comes into contact with an electrolyte, a potential difference is created at the phase boundary. This potential difference is formed due to the different electrochemical potentials of the two phases, which leads to the formation of the electric double layer. The high conductivity of the metal prevents the formation of a space charge zone inside the solid, so that the excess charge is concentrated only on the metal surface. This excess charge is compensated in terms of amount by a countercharge in the electrolyte, so that the system behaves electrically neutral towards the outside.[9, 12]
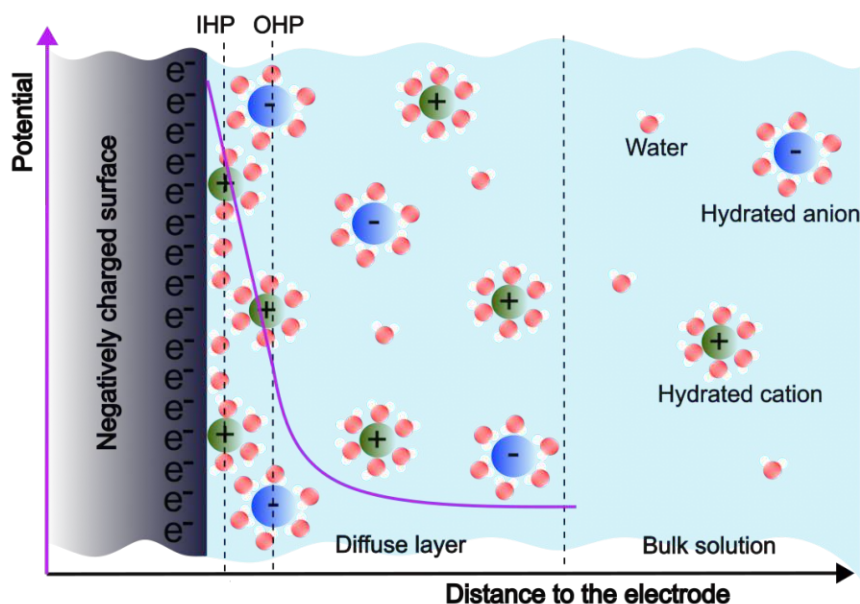

Figure 2.1: Representation of the electric double layer at the phase boundary of a negatively charged substrate. The electrical potential distribution is represented with the purple line

The contact of the electrode with the electrolyte causes the solvent molecules to align and the single ions and solvated ions to adsorb on the electrode surface. The inner Helmholtz plane is formed where there is direct contact with the metal surface. Partially solvated ions and solvent molecules are adsorbed on the electrode surface. The outer Helmholtz layer is then formed by the non-specific adsorption of fully solvated ions. These fully solvated ions are attracted to the metal surface by Coulomb forces. The inner and outer Helmholtz layers form the stationary Helmholtz layer. The following space charge zone extending into the electrolyte volume, in which the thermal movement of the ions counteracts the electrostatic forces of the surface, is called the diffuse or Gouy-Chapman layer. Thus, the electric double layer [13, 14] is the sum of the Helmholtz and the Gouy-Chapman layer, which is well represented by the the Figure 2.1. There is a relationship between current density and overpotential given by the Butler-Volmer equation 2.6. This is applicable when the passage of electrons or ions through the electrode-electrolyte phase boundary is velocity-determining.

$$i = i_0 \left\{ \exp \left[\frac{(1 - \alpha)zF\eta}{RT} \right] - \exp \left[-\frac{\alpha zF\eta}{RT} \right] \right\} \tag{2.6}$$

i_0 = Exchange current density

η = Penetration overpotential

α = Penetration factor

R = Gas constant (R = kN_A = 8.314 $Jmol^{-1}K^{-1}$)

T = Temperature in Kelvin

z = number of transferred electrons

F = Faraday constant (F = eN_A = 9.648·10^4 $Cmol^{-1}$)

2.3 Electro-crystallisation and nucleation

In this part we will discuss the topic of electrocrystallisation [15–21], because the early stages of the crystallisation are important for electrochemical metal deposition. In electrochemistry, when nucleation and crystal growth occur under the influence of an electric field, this is called electrocrystallisation. This is in fact the cathodic process that leads to metal deposition and thus to the formation of a solid crystalline phase. It is a very complex process because it consists of several dif-

ferent steps. These steps consist of chemical, electrochemical, material transport and charge transport steps, which take place as follows:

- Diffusion of the metal ions from the bulk electrolyte into the electric double layer

- Adsorption of the metal ion on the surface of the electrode

- Transfer of electrons and ions

- Partial or complete loss of the solvate envelope

- Surface diffusion of the ad-atoms

- Formation of a critical nucleus by clustering of the ad-atoms

- Incorporation of further ad-atoms into the resulting crystal lattice

- Development of crystallographic and morphological features

After migration of the solvated ions to the diffusion layer of the electrode, they move within the layer towards the electrode by diffusion. The driving force is the diffusion force resulting from the concentration gradient. When the solvated ions reach the diffuse Helmholtz layer [13, 14], the dipoles of the solvate envelope are aligned by the effect of the electric field becoming stronger. As a consequence, the ions detach from the outer, loosely bound hydration shells. The partially solvated ions enter the stationary Helmholtz layer, where a steep increase in the concentration gradient occurs and therefore also occurs in the potential gradient. From the outer to the inner Helmholtz layer, the ions lose their remaining hydration envelopes by aligning in the field and can then adsorb on the surface. The bare metal ion can be reduced to a metal atom by the electrons from the electrode. Depending on the location of the discharge, the metal atom is incorporated directly into the metal lattice of the electrode or diffuses to a suitable growth site, such as step edges or piercing points of dislocations.

Three nucleation mechanisms are assigned to electrocrystallisation. Of great importance here are, above all, intermolecular interactions between atoms. The decisive factor is always the tendency of the system to minimise its surface energy. First of all, a distinction is made between the Volmer-Weber island growth model [22–25], according to which individual crystallites are formed that grow three-dimensionally. This

model comes about when the binding energies between the substrate and atoms of the forming layer are smaller than the internal binding forces between the atoms of the new layer. If, on the other hand, the binding energies between the atoms of the forming layer and the substrate are larger than the binding energies between the atoms of the forming layer, then the two further mechanisms are more likely. From one side, the Frank-Van-Der-Merwe model [24, 25] would arise if atoms of the forming layer and substrate had similar sizes. From the other side, it would be the Stranski-Krastanov [17, 25] model if the atomic radii were different. Here, a thin epitaxial layer grows first, which changes into a three-dimensional island growth.

2.4 Electroplating

Electroplating [26, 27] is a branch of electrochemistry that deals with the electrochemical deposition of metallic layers on substrates using aqueous electrolytes. The anode and cathode are in an electrolytic bath, through which electric current is conducted. The electrons flow from the anode to the cathode. A metal is dissolved at the anode (positive pole) and then deposited on the substrate at the cathode (negative pole). Figure 2.2 shows a simplified drawing of a galvanic cell, where the anode is represented by nickel and the cathode can be any conductive material. The nickel ions in the electrolyte are reduced at the cathode and forms a nickel metallic layer at the surface of the conductive substrate (Me). Electroplating is used, among other things, to protect against corrosion, to beautify objects, to improve electrical conductivity, etc...

In practice, the electrodes are immersed in conductive liquids (bases, acids and solution of salts in water) and polarised by applying a DC voltage. By applying current, the anions move to the anode where they are oxidised and the cations to the cathode where they are reduced. Depending on the process, soluble or insoluble anodes can be used, for example. With soluble anodes, the anode is immersed in the solution of its salt. Ideally, as many ions are reduced at the cathode as are dissolved at the anode. Thus, thanks to the anode, the concentration of the electrolyte should remain unchanged. The process with soluble anodes is used, for example, in nickel plating, copper plating, zinc plating and silver plating. With insoluble anodes, the electrolyte
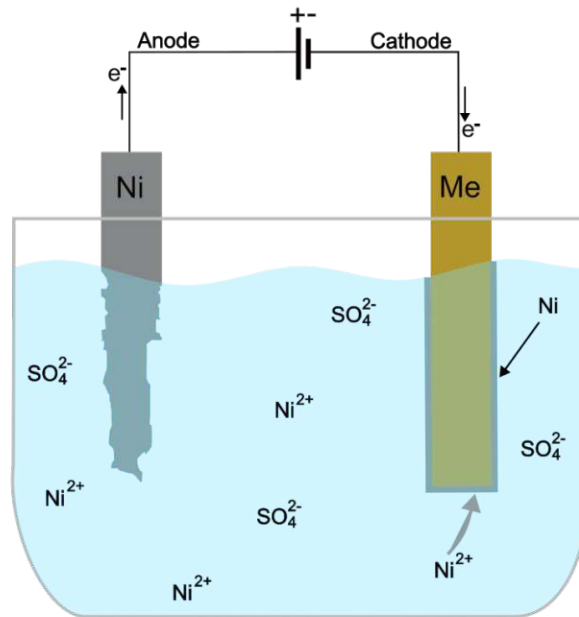
Figure 2.2: Nickel plating of a metal (Me) from a nickel sulfate electrolyte. Here the anode used is a soluble Nickel anode that electrochemically dissolve in the electrolyte to compensate the Nickel cations that were reduced at the cathode.

consists of dissolved ions of the metal to be deposited. The more the layer is deposited at the cathode, the fewer cations are available for further deposition. In order for the reduction reactions at the cathode to continue without problems, more and more metal salts must be dissolved in the electrolyte. The process with insoluble anodes is used, for example, in gold plating and zinc plating.

Faraday's law, described in equation 2.7, can be used to calculate the conversion of electrolytic deposition. The amount of a substance n deposited on an electrode is proportional to the electric charge Q that is passed through the electrolyte. The charge needed in order to electrolytically deposit any amount of a z-valent ion is described by:

$$Q = n \cdot z \cdot F \tag{2.7}$$

With

$$m = n \cdot M \tag{2.8}$$

and

$$Q = I \cdot t \tag{2.9}$$

The equation can be redefined by:

$$m = \frac{M \cdot I \cdot t}{z \cdot F}$$ (2.10)

M = Molar mass of the substance
m = mass of the substance
I = applied electric current
t = total time during which the current was applied
F = Faraday constant.
In order to be able to deposit a layer with good properties and efficiently, various parameters must be taken into account. These are:

- bath temperature

- duration of the deposition

- current density

- pH value of the bath

- distance between the electrodes

- composition of the bath

- degree of contamination of the bath

- degreasing of the substrate etc...

Some of these parameters will be critical, when it comes to up-scaling of the electrodeposition in the galvanic industry. The bath temperature, the pH-value, the cleanliness of the substrate and degree of contamination of the bath are the parameters that induce the most problems in the large equipment used in industry. Some components, for example, may precipitate at higher temperature and pH. This can obturate the equipment. In the industry they use a large amount of substrates. These substrates should be clean because otherwise they will contaminate the bath with a huge amount of dirt. For this dissertation we will focus on the bath composition and especially on one polymer additive that is used as a leveller.

2.5 Polymers in solution and adsorption

To produce a smooth and bright zinc layer, we will ingrate a polyquaternary ammonium polymer into the plating bath as the leveller. The polymer behaviour in aqueous solutions has to be taken into account. Polymers cannot enter the gas phase due to their high molecular mass. Therefore, the study of polymers in solutions [28, 29] is a very important topic in the research of macromolecules. In this work, how polyquaternium 2 behaves in its aqueous environment and how it adsorbs into this aqueous environment on the metal surface plays an important role.

A specific polymer can dissolve well in some solvents, while it dissolves only partially or not at all in other solvents. With good solvents, high concentrations (up to 100%) of polymers can be dissolved without changing the uniformity and clarity of the solution. With mediumquality solvents, only a limited amount of polymer can be dissolved in them. If a bad solvent is miscible with the good solvent, it would lead to precipitation of the polymer when added to the polymer solution.

The dissolution of polymers [29, 30] takes place in two steps. First, the solvent molecules slowly diffuse into the polymer and form a swollen gel. Then the gel dissolves gradually to form the solution. The dissolution can be accelerated by stirring. The solubility depends on the temperature of the solution, the nature of the solvent, the crystallinity and the structure of the polymer. An interesting aspect of polymer dissolution is that polymers form random coils in solution unless the main chain is rigid. The size of the molecular coil is determined by the interaction between the polymer and the solvent. A good solvent will cause the coils to be relatively extended, while a poor solvent leads to the formation of smaller coils. This is because in a good solvent there is good contact between the polymer and solvent. While there is little contact or no contact at all in a poor solvent. In order for a monomer to have as much contact surface as possible with solvent molecules, the polymer must stretch slightly. This results in a more stretched chain conformation compared to the ideal solvent, which can be described mathematically by a random path that does not intersect itself (self-avoiding random walk). The radius of gyration in this case can be written as:

$$R_g = \frac{I_s}{\sqrt{6}} \cdot \eta_s^v \tag{2.11}$$

The fundamental thermodynamic equation used to describe these systems relates the function of the Gibbs free energy G with the enthalpy H and the entropy S. Thus, if the Gibbs free energy of the solution G_{AB} is smaller than the sum of the Gibbs free energies of the individual components G_A and G_B, the substance dissolves homogeneously in the solvent.

$$\Delta G = G_{AB} - (G_A + G_B) < 0 \tag{2.12}$$

$$\Delta G = \Delta H - T\Delta S \tag{2.13}$$

The Flory-Huggins theory is a mean-field theory that [28, 29, 31] explains quite well the thermodynamics of the mixture of a polymer with a specific solvent. Here, the free energy of the polymer-solvent system is compared before mixing and after mixing.

We cannot talk about polymers in solutions without mentioning their adsorption at a solid-liquid interface. This aspect is important for the understanding of this work. When a polymer adsorbs on a certain surface, it can assume different conformations depending on the following parameters: the solvent, the number of repeating units, the length of the monomer and the total area available for adsorption. The radius of the volume that the polymer has at the surface is defined by the Flory Radius R_F in equation 2.14.

$$R_F = l_s \cdot \eta_s^v \tag{2.14}$$

η_s is the number of monomers per polymer chain, l_s is the length of a monomer and v is the Flory constant. The Flory constant indicates how good a solvent is. For this work, the Flory constant has a value of 3/5, as water is a good solvent for polyquaternium 2. Therefore, there are two main conformations [32, 33] that the polymer can adopt at the surface of the substrate depending on the density: the mushroom and the brush conformation (See Figure 2.3). The mushroom conformation takes place at low adsorption density, i.e. when the distance between the side chains of adsorbed molecules D is greater than R_F. However, when R_F is greater than D, the brush conformation takes place due to
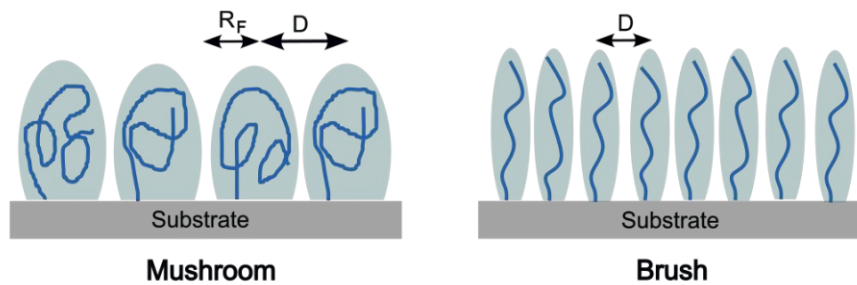
Figure 2.3: Mushroom and brush regimes of a polymer adsorbed at the surface of a planar substrate.

the high adsorption density.

2.6 Zinc electroplating

Electroplating of zinc is an industrial process used to produce a protection layer on a ferrous substrate. Zinc deposition and dissolution [34–36] processes are widely studied. Owing to its more negative standard electrode potential (in contrast to iron) zinc will corrode preferably over the steel to produce a sacrificial protection of the substrate [37–40]. Zinc deposition is also utilised in the growing fields of novel rechargeable battery design [41, 42] and CO2 reduction [43]. For large-scale applications a central hurdle of the electroplating process is control of the local deposition rate. In several industries, complex substrate geometries result in high/low field regions with significantly varying local deposition rates. Controlling and steering the local process can provide real benefits to manufacturers, in particular via targeted control of deposition rates through an inhibition at high current densities and an acceleration at low current densities. This results in a more even thickness distribution and a smooth and bright appearance of the zinc layer.

Due to its amphoteric property, zinc is soluble in both alkaline and acidic conditions, as well as novel neutral [44], and non-aqueous electrolytes [45]. For electroplating this enables the deposition of zinc from both alkaline and acidic electrolytes. There are three main electrolytes used: alkaline cyanide, alkaline non-cyanide and acidic electrolytes [26, 46]. Nowadays alkaline cyanide based chemistry is rarely used because of its toxicity. Alkaline non-cyanide electrolytes were developed as non-toxic alternatives and are the focus of the present work.

A typical alkaline electrolyte is prepared by dissolving zinc oxide in sodium or potassium hydroxide solution to form $[Zn(OH)_4]^{2-}$ (zincate) complexes. Jelinek et al. show that the complex $[Zn(OH)_4]^{2-}$ is formed in these electrolytes [46]. Spectroscopy measurements also provide evidence that only $[Zn(OH)_4]^{2-}$ is formed when preparing alkaline zinc electrolytes [47, 48]. Also measuring the redox potential of zinc in strongly alkaline electrolyte further supports the formation of $[Zn(OH)_4]^{2-}$ [49]. It is important to note that the formation of the tetrahydroxo zincate complex only appears in highly concentrated alkali hydroxide solution (an excess of hydroxide ions is needed). In contrast to this the formation of $[Zn(OH)]^+$, $[Zn(OH)_2]$ or $[Zn(OH)_3]^-$ is favoured in less alkaline conditions [50].
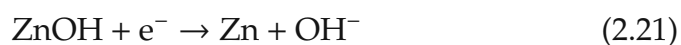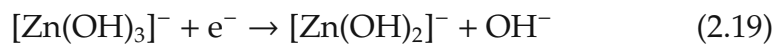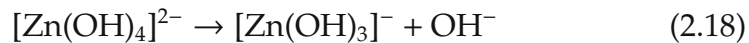
The mechanism of Zn-deposition is debated controversially. Some authors claim that the zinc reduction happens as a one-step electron transfer reaction [51, 52]:

$$Zn(OH)_2 + 2e^- \rightarrow Zn + 2OH^- \qquad (2.15)$$

while others propose a two electron process as follows [46]:

$$Zn(OH)_2 + e^- \rightarrow ZnOH + OH^- \qquad (2.16)$$

$$ZnOH + e^- \rightarrow Zn + OH^- \qquad (2.17)$$
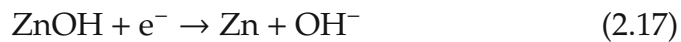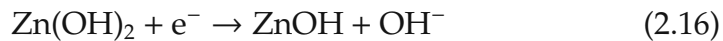
Indeed other studies show that the reaction of the zinc electro reduction is more complex and may proceed through a four-step mechanism starting from the tetrahydroxo complex as follows [53–55].

$$[Zn(OH)_4]^{2-} \rightarrow [Zn(OH)_3]^- + OH^- \qquad (2.18)$$

$$[Zn(OH)_3]^- + e^- \rightarrow [Zn(OH)_2]^- + OH^- \qquad (2.19)$$

$$[Zn(OH)_2]^- \rightarrow ZnOH + OH^- \qquad (2.20)$$

$$ZnOH + e^- \rightarrow Zn + OH^- \qquad (2.21)$$

Although alkaline baths nowadays are environmentally benign, they have disadvantages, specifically the formation of powdery, dark or

16

spongy zinc layers. To overcome these problems, and to improve the plating performance, additives can be utilised for moderating the crystal growth [4, 5, 56]. A number of additives show excellent performance. For instance Ortiz-Apericio et al. [6] show a beneficial influence of vanilin and anisaldehyde on the electrochemical deposition and the layer morphology of a Zn-Co alloy. Polyvinyl alcohol addition also results in a grain refinement during the deposition [4]. Similarly, quaternary ammonium compounds (for example: tetraethylammonium hydroxide, tetrabutylammonium hydroxide, nicotinic acid and N-benzyltriethylammonium) can effectively inhibit dendrite formation of zinc [7].

In the industry they have been using poly quaternary ammonium compounds without knowing what is really happening at the interface of the working electrode during the metal deposition. In this work we are going to study the influence of a such a compound specially polyquaternium 2 (Poly[bis(2-chloroethyl) ether-alt-1,3-bis-[3-(dimethylamino)propyl]urea] quaternized) in the electrodeposition mechanism of zinc. Several methods such as cyclic voltammetry, QCM-D, XPS, LEIS and AFM are used to understand the polymer moderated deposition of zinc in a alkaline bath. We will be able to understand the phenomenon that happens at the interface during the polymer moderated deposition. Those investigations will also lead to the synthesis of a better working poly quaternary ammonium polymer.

3 Materials and methods

3.1 Chemical and materials

The zinc oxide (99.7% purity) as well as the NaOH solution (50%) and the Urea were purchased from VWR. The polyquaternium 2 (62wt. % in water), the 2-bis(2-chloroethoxy)ethane as well as the N,N-dimethyl-aminopropylamine were purchased from Sigma Aldrich. All chemicals were used as received without further purification.

The alkaline non-cyanide zinc electrolyte was prepared by dissolving the zinc oxide in NaOH solution and using deionized water to achieve the desired concentration. The concentration in the bath is 3.8 M for the NaOH and 0.2 M for the zinc. The polyquaternium 2 in the electrolyte is adjusted to 0.1wt. %.

The Ultrafiltration membrane were from the company MICRODYN-NADIR for the 10kDa and 20kDa (NADIR UP010 P and NADIR UP020 P) and from Synder Filtration for the 1000Da (XT (PES 1000Da)). The Dialysis (ultrafiltration) equipment used was the MMS Mem Tester from the Company MMS AG Menbrane Systems.

The test sheets used for the Hull cell experimentation are steel sheets from the company Pauly Stahlhandel in Germany. This is exactly the ST2 hull cell sheet made of steel with the dimensions $0.30 \times 70 \times 100$ mm. The sheets are electrolytically matt galvanised with a zinc layer of approx. 2 to 3 μm. Before use the sheets are dipped in a pickling solution of 31% hydrochloric acid to remove the protective layer and then rinsed.

The samples for the IR measurement were prepared before the experiments by freeze-drying to remove any interfering moisture. 1λ fused silica uncoated glass (12.5 mm diameter, 2 mm thickness) used as window in the Hull-cell for the Laser interferometry was purchased from Edmund Optics, while the Glue used to fix the window to the viewport was the optical glue EPO-TEK 302-3M that we purchased from the company Epoxy Technology. The Hull-cell for the inter-

ferometry experiment was printed with the 3D-printer Ultimaker 2+ Connect from the company Ultimaker B.V. and the printing material was a Formfutura-Centaur polypropylen filament with a diameter of 2.85 mm that we purchased from the company Filamentworld.

3.2 Methods

3.2.1 Cyclic voltammetry (CV)

The zinc layer was deposited during cyclic voltammetry in a bulk electrochemistry on a gold model surface using a GAMRY potentiostat/galvanostat/ZRA (interfaces 1010 E). During the experiments the solutions were bubbled continuously with argon. The working electrode was a molecularly smooth gold surface prepared by template stripping from 100 nm gold deposited on mica [57] with a geometrical area of 1 cm^2 and an RMS roughness well below 1 nm over several cm^2. The flat, glass supported electrode was contacted with a gold wire. Experiments were carried out in a three-electrode setup in a cylindrical PEEK cell with platinum mesh as counter and Ag/AgCl electrode (in 3 M KCl, in a Luggin capillary) as the reference. For each experiment fresh gold electrodes were stripped shortly before experiment, and the working electrode was electrochemically further preconditioned in a 0.1 M NaOH solution by potential cycling (between -0.3 to 0.3 V vs. Ag/AgCl). All measurements were made at a rate of 10 mV/s. The stability of the experiment was determined by measuring the OCP of the Ag/AgCl electrode over a time period of 6h.

3.2.2 Cyclic voltammetry in QCM-D cell

The zinc deposition happened in an electrochemical QCM-D cell on a gold surface using a GAMRY potentiostat/galvanostat/ZRA (interfaces 1010 E). The electrolytes were prepared as above and stored in plastic containers. During the experiment a Teflon beaker was used and the solution was bubbled constantly with argon during experiments. The equipment (a Qsense E1) and the gold-coated quartz sensors (with an RMS roughness below 1 nm) were purchased from Biolin Scientific and used in the Qsense electrochemistry module. The experiments were performed at 24°C under flow conditions and the fifth over-

tone was used for the data analysis, with the Sauerbrey equation to calculate the mass deposited. For the zinc and zinc with polyquarternium 2 electrolytes the Sauerbrey equation is appropriate [58], for the polyquarternium 2 and background electrolytes the criterion is met to differing extents and therefore the mass should be treated as indicative rather than quantitative. For the cyclic voltammetry part a platinum sheet and an Ag/AgCl electrode (in 3 M KCl) were used respectively as counter and reference electrodes. Every gold sensor was electrochemically polished in a 0.1 M NaOH solution before starting the experiment and used for one zinc deposition experiment only. 10 cycles were measured and the last 3 cycles are plotted in this work. Transient chronoamperometric measurements were also made using the same preparation protocol and returned to a dissolution potential between potential steps.

3.2.3 Cyclic voltammetry for AFM

The zinc layer was deposited at room temperature during chronoamperometry on a gold model surface using a PalmSense4 potentiostat. During the experiments the solutions were bubbled continuously with argon. The working electrode was a molecularly smooth gold surface prepared by template stripping from 100 nm gold deposited on mica [57] with a geometrical area of 1 cm^2 and an RMS roughness well below 1 nm over several cm^2. The flat, glass supported electrode was contacted with a gold wire. Experiments were carried out in a three-electrode setup in a cylindrical PEEK cell with platinum mesh as counter and Ag/AgCl electrode (in 3 M KCl, in a Luggin capillary) as the reference. For each experiment fresh gold electrodes were stripped shortly before the experiment, and the working electrode was further electrochemically preconditioned in a 0.1 M NaOH solution by potential cycling (between -0.3 to 0.3 V vs. Ag/AgCl at a rate of 100 mV/s). Each layer was deposited using chronoaperometry at fixed potentials for 30s.

3.2.4 X-ray photoelectron spectroscopy

Gold substrates were prepared as for the bulk electrochemistry and samples were prepared in polyquarternium 2 solution (removed at peak PQ2, approached by linear sweep voltammetry at 10 mV/s scan

rate), zinc with polyquarternium 2 prepared both under the same conditions at the PQ sample and removed at -1.62 V at the beginning of the zinc deposition peak and in the zinc electrolyte after a CV (0.05 V to -1.5 V, 10 mV/s) removed at 0 V. Chemical composition and chemical states of the surface were determined using the Axis Supra (Kratos Analytical) spectrometer. No charge neutralization was used. XPS spectra were shifted with respect to gold at 83.95 eV. Spectra were taken with a resolution of 0.1 eV and a pass-energy of 160 eV. All spectra were fitted using reference compounds from the NIST database.[59, 60]

3.2.5 Surface preparations for AFM

We used Nordland optical adhesive 81 to attach the sample to the AFM specimen disc. Electrochemically deposited zinc surfaces were prepared as described below before being gently rinsed with water and finally dried with nitrogen before imaging in the AFM. For the experiment with polyquarternium 2 on mica (from the full alkaline, zinc electrolyte as prepared above) we deposited a drop (10 μL) of the solution on a freshly cleaved mica piece (grade V1) and rinsed it off gently with Milli-Q water after approximately 5 minutes it was then dried at 60 °C before imaging in the AFM. The sample was then kept in a petri dish at room temperature for 3 days prior to further imaging.

3.2.6 Atomic Force Microscopy

The atomic force microscopy images were recorded in air at room temperature using an Asylum Research Cypher ES Atomic Force Microscope. In tapping mode we used a silicon cantilever Tap300-G from budget sensors with a resonance frequency of 300 kHz and a nominal force constant of 40N/m. The volumes of the polymer islands were determined as histograms of grains with a minimum height threshold of 1 nm using the Gwyddion software.[61]

3.2.7 Low energy ion scattering

High sensitivity-low energy ion scattering (HS-LEIS) measurements were performed using an ION-TOF Qtac[100] spectrometer (IONTOF, Germany) with ^{4}He$^+$ at 3 keV as primary ion at an incident angle of 0° and scattering angle of 145°. The measurement area was 1.5 x

1.5 mm^2. The sputter depth profiling was performed with a sputter beam consisting of ^{40}Ar$^+$ 500 eV and 2 keV, respectively, at an incident angle of 59° and a sputter area of 2.5 x 2.5 mm^2. The HS-LEIS signals for Zn and Au were quantified against metallic Zn and Au reference standards, with the residual ascribed to the elements H, C, N, O, and Na. An approximation of the depth per sputter cycle was performed via the software ITCalculator (IONTOF) using the respective sputter yields of the elements as well as the measurement parameters. This has resulted in a step size of 0.1-0.15 nm for Ar$^+$ 500 eV, while no value was determined for Ar$^+$ 2 keV due to the large range of variation.

3.2.8 Gel permeation chromatography (GPC)

The GPC was carried out by the company PSS polymer standards service GmbH. The following conditions were applied for the analysis:

- Eluent: 0.1 M NaCl and 0.1 vol.% TFA in deionised water.

- Pre-column: PSS NovemaMax, 5μm, Guard, ID 8.0 mm x 50 mm

- Columns: PSS NovemaMax, 5μm, 100 Å, ID 8.0 mm x 300 mm
  PSS NovemaMax, 5μm, 100 Å, ID 8.0 mm x 300 mm
  PSS NovemaMax, 5μm, 100 Å, ID 8.0 mm x 300 mm

- Pump: PSS SECcurity 1260 HPLC pump

- Flow rate: 1.0 ml/min

- Injection system: PSS SECcurity 1260 Autosampler

- Injection volume: 20 μl

- Sample concentration: approx. 5g/l

- Temperature: 35°C

- Detectors: PSS SECcurity 1260 RI detector

- Data Interpretation: PSS-WinGPC UniChrom Version 8.31

Several dextran or pullulan samples with known molecular weights were measured and a conventional calibration was created from the measured data. The calculation of the molar mass distributions and the mean values of the samples was carried out computer-aided by means of the strip method based on the dextran/pullulan calibration curve.

3.2.9 Infrared spectroscopy

The IR measurements were carried out using a Bruker Equinox 55 with a diamond ATR unit. The sample was placed on the ATR unit and fixed by means of the measuring head. The spectra were recorded from 180 individual measurements in the range from 4000 to 400 cm⁻1 and referenced against a background measurement.

3.2.10 Laser Interferometry

The Laser interferometry experiments were carried out using the interferometric displacement sensor IDS3010 with the Sensor Head D4/F17 (working range up to 65 mm) from attocube systems AG. The sensor head has a diameter of 4 mm and a length of 11.5 mm.

3.2.11 Ultrafiltration

The equipment used was the MemTester (Machine Nr:20122) from the company MMS AG Membrane Systems. It is a high pressure stainless steel stirred cell, that works with compressed nitrogen gas. The experiment was carried out at room temperature. For more information to the device visits the website of MMS AG Membrane Systems [62].

4 Adsorption and diffusion is moderated by polycationic polymers during electro deposition of zinc

The following chapter is a reproduction of my published article that appears in ACS Applied Materials and Interfaces [63]. No additional permission was required as the paper is licensed under a Creative Commons Attribution license CC-BY.

4.1 Introduction

Already, in 1972 Diggle and Damjanovic [64] realized the effect of quaternary alkyl ammonium salts on the dendrite formation during electrocrystallization of zinc and argued that two mechanisms are active. On the one hand a physical blocking (steric) of the surface by the adsorbed inhibitor moderates deposition at highly catalytic sites [65]. On the other hand the specific adsorption of the quaternary compounds modifies the diffuse layer, so that deposition kinetics, i.e. the position of the reaction planes is modified. The effect of specific adsorption of moderators was further confirmed by Oniciu and Mureşan [56].

While it seems clear that adsorption of molecules can effectively moderate metal deposition, little is known about the molecular mechanism and moderation mechanism of other moderators such as polymers during electroplating.

The aim of this work is to fundamentally understand the effect of organic compounds, especially polyquaternary ammonium polymers, on the electro deposition of zinc. This work investigates the behaviour of Polyquaternium 2 (PQ) as an additive for the alkaline zinc electrolyte, with the aim to unravel the mechanism by which it controls zinc depo-

25

sition. Here cyclic voltammetry and quartz crystal microbalance with dissipation (QCM-D) measurements were performed to understand the adsorption mechanism and kinetics during the metal deposition, and the role of the polymer in the alkaline electrolyte. Knowing this information can help to improve electrolyte systems both in terms of the material properties of the electroplated layer produced and their environmental impact.

4.2 Results and discussion

In this work we studied the influence of polymer additives on zinc deposition from the alkaline zinc bath using both electrochemistry (cyclic voltammetry) and QCM-D measurements. The key questions that we try to answer are: how does the polymer influence the deposition mechanism, and how does this enable deposition of a thin, smooth, and bright zinc layer with optimized thickness?

Four electrolytes have been analyzed as shown in Figure 4.1: The background electrolyte NaOH (labeled BE), a solution of 0.1% polyquaternium 2 in NaOH (PQ), zinc electrolyte without polyquaternium 2 (ZN), and zinc electrolyte with 0.1% polyquaternium 2 (ZP). The characteristic cyclic voltammograms in the cathodic region on a gold electrode are compared. These data reveal a number of interesting aspects as follows.

Figure 4.1 BE shows the electrochemical behavior of a gold electrode in the NaOH electrolyte with two characteristic reduction peaks labeled BE1 and BE2. The first cathodic peak BE1 at −1.14 V vs Ag/AgCl is attributed to the adsorption of cations (H^+ and Na^+) at the electrode interface. At a potential of about −1.3 V the hydrogen evolution reaction (HER) starts to dominate.

In contrast for PQ, also shown in Figure 4.1, the CV indicates five peaks (PQ1, PQ2, and PQ3 in the cathodic sweep and PQ4 and PQ5 in the anodic sweep). The peaks PQ1 at −0.92V and PQ2 at −1.12 V vs Ag/AgCl can be attributed to the electrosorption of the polymer. The intensity of PQ1 is smaller and may characterize low-molecular-weight compounds in the solution and residual oligomers formed during the synthesis. Alternatively, the combination of both peaks may be interpreted as an initial electrosorption with low coverage, where the polymer remains in a mushroom regime, while the second peak may
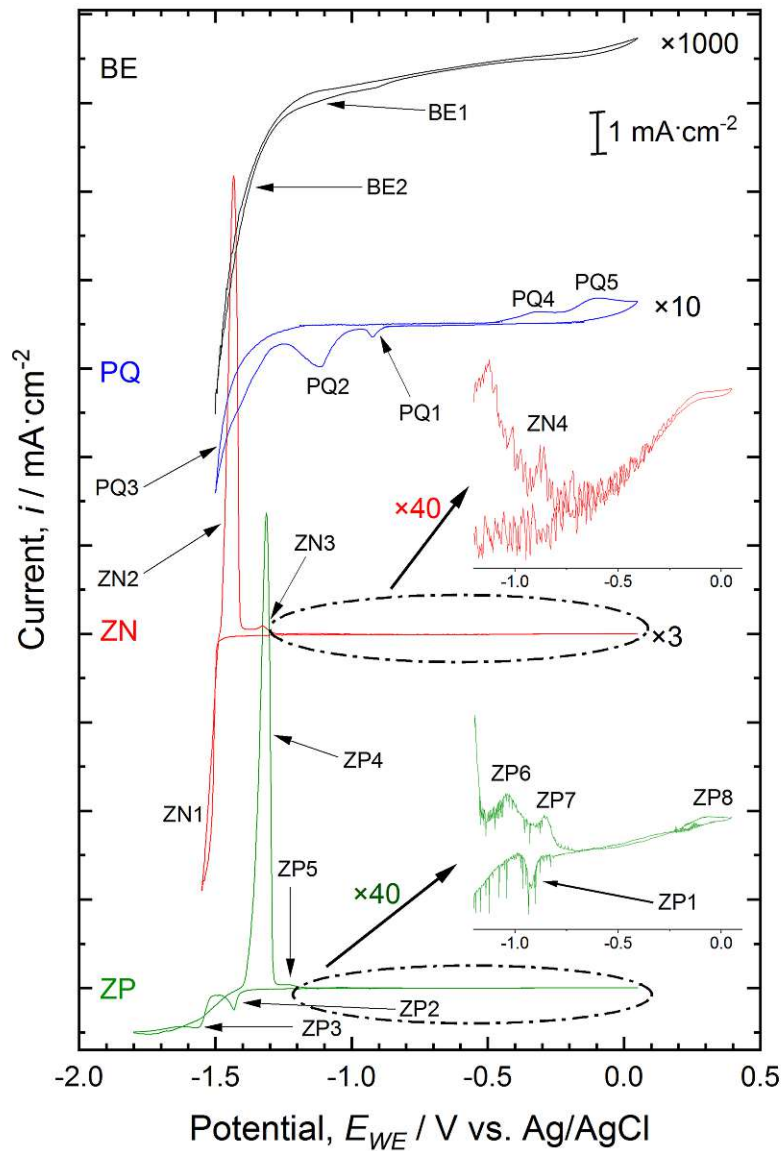
26

Figure 4.1: Full cyclic voltammogram (CV) of the electrolytes analyzed during this work. BE is a 100 times magnification of the CV of NaOH. PQ is a 10 times magnification of the CV of the polyquaternium 2 dissolved in NaOH (0.1% solution). ZN is a 3 times magnification of the CV of the zinc electrolyte containing no polyquaternium 2. ZP is the CV of the zinc electrolyte with polyquaternium 2

indicate a collapse of the adsorbed molecules into a more dense packing.

The adsorption or grafting of polymer chains on to a planar solid-liquid interface is a well-studied phenomenon [32, 66]. Briefly, there are two main configurations or regimes depending on the density. At low surface density the mushroom regime describes the grafting of polymer chains to the interface without overlap between neighboring chains. This is possible when the surface density of anchored polymer Γ is smaller than $1/R_F^2$, where R_F is the Flory radius. Each chain is isolated from its neighbors with the average distance between grafting points larger than the radius of gyration. When the chains are adsorbed at high densities, the probability of obtaining a brush structure for the resulting layer is very high, especially when the neighboring chains are so close that they can overlap with each other.

Interestingly, also the HER is significantly altered and indicates an additional shoulder at about −1.35 V (PQ3). We interpret this as a moderation of the HER by the adsorbed polymer. Moderation is likely linked to a lower number of adsorption positions of water due to competitive polymer adsorption and a related change of the reaction mechanism and/or kinetics of the HER. This is an interesting insight and demonstrates that the positively charged polymer can effectively compete with or rather modify the kinetics of the HER. In the anodic sweep, the peaks PQ4 and PQ5 can be attributed to desorption of polyquaternium 2. This is obviously a highly nonideal electro(de)sorption process with a considerable overpotential, considering the potentials of the electrosorption peaks (PQ1 and PQ2). This is not unexpected for large molecules such as polymers [67, 68].

Comparing the pure zincate solution, ZN, in Figure 4.1 with the two other reference solutions shows one significant cathodic peak ZN1 and three anodic peaks ZN2, ZN3, and ZN4 at −1.43, −1.33, and −1.13 V vs Ag/AgCl, respectively. ZN1 is indicative of a competitive zinc deposition and HER. Interestingly, also the HER is shifted in the ZN solution and starts at −1.48 V vs Ag/AgCl, which is significantly more negative in comparison to BE and PQ. This indicates that the zincate in solution may result in an interfacial adsorption layer, i.e., an electric double-layer structure in this case, that modulates the hydrogen adsorption and consequently the HER kinetic pathways by competitive adsorption. The anodic peak ZN2 indicates the corresponding Zn

dissolution peak during the anodic sweep.

Including both the polyquaternium 2 and the zincate in the ZP electrolyte results in significant changes to the cyclic voltammogram in Figure 4.1. Here, we find three cathodic peaks with those related to the zinc deposition, ZP2 and ZP3, appearing at significantly more cathodic potentials of −1.43 and −1.56 V vs Ag/AgCl, respectively, and five anodic peaks with the main zinc dissolution peak, ZP4, at −1.30 V vs Ag/AgCl. Compared to the zincate solution ZN, the Zn deposition is obviously actively moderated.

For interpreting this result, we will need to consider, first, how the polymer structure changes in the two different alkaline solutions and how it enables an effective Zn deposition. In alkaline solutions the polyquaternium polymer will be positively charged, as the quaternary amine is charged at all pH levels. This charge on the polymer will be screened by coion absorption (e.g., OH^-) into the polymer. In turn, the polymer will remain in a random coil structure, with a typical radius that depends on the contour length of the individual coils and the solubility. As the solubility is quite good, the radius can be estimated by using the Flory radius $R_F \sim l_s \eta_s^{0.6}$, where η_s is the number of segments and l_s the length of a segment [69]. As explained above, the R_F is the typical distance to which polymers can adsorb at surfaces without significant compacting and brush formation. If zincate is present, the zincate can easily coabsorb into the polymer, in an effective competition with hydroxide ions, to screen the charge of the polymer. There are two motifs that can result in significant uptake of zincate into an amine-based polymer. First, positively charged amine groups can interact with the negatively charged zincate, and second, amines can complex with the zincate directly. Given the quaternary amine structure of PQ, the first possibility seems more likely, while complexation is impossible with quaternary amines [70, 71]. This coabsorption of zincate into the polymer enables its approach to a negatively charged surface, directly into the inner sphere of the electric double layer. Essentially the electrostatic penalty is lifted, enabling a controlled approach to the negatively charged surface at deposition potentials.

Now, considering such a Zn-loaded polymer structure, the CV peaks may be described as follows: the weaker positive charge of the polymer structure leads to corresponding electrosorption peak, ZP1, at −0.92 V to have a much lower current than in the PQ solution. ZP1

also appears to form a couple with ZP7 at −0.86 V. Consistent with this interpretation is the broad peak, ZP8, at ~ −0.06 V, which would correspond to PQ5, attributed to electrodesorption of the polymer in the PQ solution. The peak at ZP2 may hence indicate the deposition of the zinc that is absorbed within the positively charged polymer coil. The overall only weakly positively charged polymer aggregate enables an effective approach of zincate to the surface, without a significant electrostatic penalty. The peak structure clearly indicates a process that quickly depletes, which is in line with Zn depletion of the surface bound polymers. This first Zn deposition peak deposits an initial Zn layer at a 100 mV more anodic potential compared to Zn deposition in ZN solution. This is further indicative of a significant overpotential reduction for the Zn deposition, which supports a polymermediated activation of the zincate complex by coabsorption into the amine polymer coil. In addition, the second rise and plateau of the cathodic deposition current, at ZP3, is consistent with a Zn deposition that is moderated and rate limited by diffusion of zincate through the adsorbed and surface bound polymer. In particular, considering that this current levels and only weakly depends on the potential below about −1.6 V, a diffusion-controlled process moderation through the polymer is active in the combined system. The polymer is an effective surface coating that diffusion limits the zinc deposition by structural features of the polymer and its effective integration into the electric double layer at negative potentials.

Also the Zn dissolution peaks ZP4, ZP5, and ZP6 are shifted to more anodic potentials compared to dissolution from the ZN electrolyte, ZN2, ZN3, and ZN4.

XPS spectra in Figure 4.2 further support the mechanism of an initial loaded polymer bringing the zincate to the surface. Upon comparison of the ZP sample removed at the polymer deposition potential (polarized to a potential equivalent to peak PQ2) with the other ZP and ZN samples, there is a peak at a binding energy far lower than any reported in the NIST database for either metallic or zinc oxide or hydroxide.

Therefore, in Figure 4.2 and Table 4.1 we assign the peaks at 1017 and 1040 eV to zinc located within the polymer environment.

There is a coexistence with the oxide which could have formed between preparation and measurement. There was also little evidence to suggest alloying of the zinc with the gold substrate [72] following
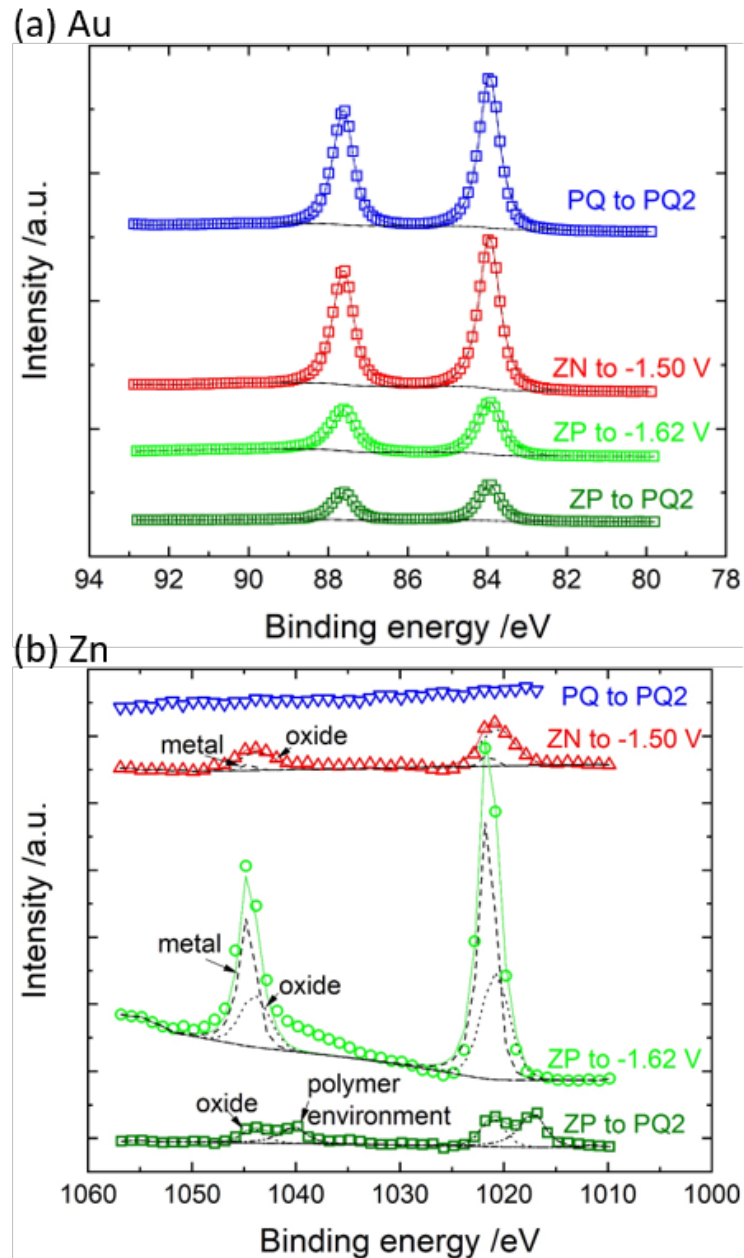
Figure 4.2: XPS spectra for (a) Au $4f_{7/2}$ and $4f_{5/2}$ and (b) Zn $2p_{3/2}$ and $2p_{1/2}$ electrons for gold electrodes in three different electrolytes: PQ polarized to the potential of peak PQ2, ZN polarized to -1.5 V (the start of deposition) but then removed at 0 V, and ZP polarized to and removed at both -1.62 V (the start of deposition) and the equivalent potential of peak PQ2. In (a) only metallic gold peak characteristics were required to fit the data. In (b) both metal and oxide characteristics are found for the ZN and ZP samples taken to deposition potentials, whereas the ZP sample polarized to the PQ adsorption potential exhibits an oxide peak and another assigned to the Zn species in the polymer environment.

Table 4.1: Peak positions for fits to the Zn $2p_{3/2}$ and $2p_{1/2}$ XPS Spectra.

position(eV) Zn $2p_{3/2}$ | $2p_{1/2}$	metal	oxide	polymer environment
PQ to PQ2 ZN to -1.5 V	1021.29|1044.31	1020.64|1043.75	
ZP to PQ2		1021.03|1044.03	1017.14|1040.14
ZP to -1.62 V	1021.48|1044.54	1020.83|1043.94	

polarization to deposition potentials in either ZN or ZP electrolytes.

While CVs and XPS already provide a detailed insight into the electrochemical mechanism at play, QCM-D experiments can further support arguments discussed above. In the following paragraphs, we discuss electrochemical QCM-D measurements with similar solutions and surfaces. This provides a direct view on the mass deposition during the zinc electroplating process. Figure 4.3 shows the variation of the current and the deposited mass and dissipation during cyclic voltammetry for all electrolytes examined for a potential window from −0.4 to −1.2 V vs Ag/AgCl, where no zinc is yet deposited. This is thereafter termed nonreactive cycling in the polymer adsorption/desorption region. Figure 4.4 goes further into the cycling of dissipation observed in ZP electrolyte. Later Figure 4.5 shows QCM-D data for active zinc deposition (with bulk deposition) from the zinc electrolyte without (ZN) and with polyquaternium 2 (ZP). The presented data indicate a number of interesting results as follows.

First, during nonreactive cycling with the background electrolyte, NaOH (Figure 4.3a-BE), the mass adsorbed to the gold surface increases and decreases, mirroring the trend of the current measured during cyclic voltammetry. The turning points coincide with those of the applied potential at −1.20 and −0.40 V vs Ag/AgCl. The changes are overlaid on top of a significant initial adsorption that is seen when cycling first begins. Here, the corresponding sharp decrease back to the baseline mass at OCP is seen in the figure after the final cycle finishes and the potential returns to OCP. The ions available in solution are Na^+ and OH^-; therefore, the mass increase must be attributed to charge regulation of these ions within the electric double layer (EDL). Upon cathodic polarization, the increasingly negative surface charge, σ, of the gold is compensated by an increasing adsorbed mass of sodium ions, as seen in the plot. Owing to the dissipative changes in the BE

data, a full kinetic network model would be required to interpret the full viscoelastic behavior of the EDL.

Second, the PQ mass vs potential characteristic is shown in Figure 4.3a-PQ. The trend is similar compared to the BE with turning points at the applied potential -1.20 and -0.40 V vs Ag/AgCl. There are two notable differences compared to BE. First, the data also show a significant plateau region at anodic potentials, and no significant jump is observed upon switching back to OCP. This indicates that the positively charged polymer is likely physisorbed at all potentials, limiting the need for compensating any surface charge with sodium from the EDL. Second, the increase and the decrease of the adsorbed mass have a slightly steeper slope of mass vs potential. The slope change may indicate denser packing of polymers, with the higher physisorbed polymer mass reflected in the increased slope.

Third, Figure 4.3a-ZN describes the behavior of the zinc electrolyte without polyquaternium 2. As can be seen, compared to the first two solutions, the characteristic is completely different. There are flat plateau regions at more anodic potentials. The significant difference in mass between the more anodic and cathodic potentials indicates that the zincate electrolyte forms a significantly different electric double layer compared to the simple EDL charging observed in pure NaOH (BE). At a critical potential of about -1 V ions may compact at the inner Helmholtz plane of the electric double layer, increasing the effective mass on the electrode, while no additional stepwise current flows.

Finally, Figure 4.3a-ZP corresponds to the current and mass plots for the zinc electrolyte with polyquaternium 2 (ZP). Here we find a completely different characteristic. Three peaks are visible for every cycle. The mass plot (thin line) appears to be a qualitative addition of effects seen for both the zinc electrolyte without polymer (ZN) and the polymer solution (PQ). Similar to ZN, we see an initial plateau followed by a steep mass increase at a critical potential of about -1 V (labeled with ZP4). After steep increase, the mass first decreases slightly and then follows the trend of the adsorbed polymer.

We interpret the steep increase at -1 V as the proposed initial electrosorption of a zincate-loaded polymer. In contrast to the pure polymer, we find a subsequent short drop in mass indicating an initial electrosorption and a subsequent depletion of the polymer. Afterward, a mass increase similar to that of the polymer solution, and no plateau
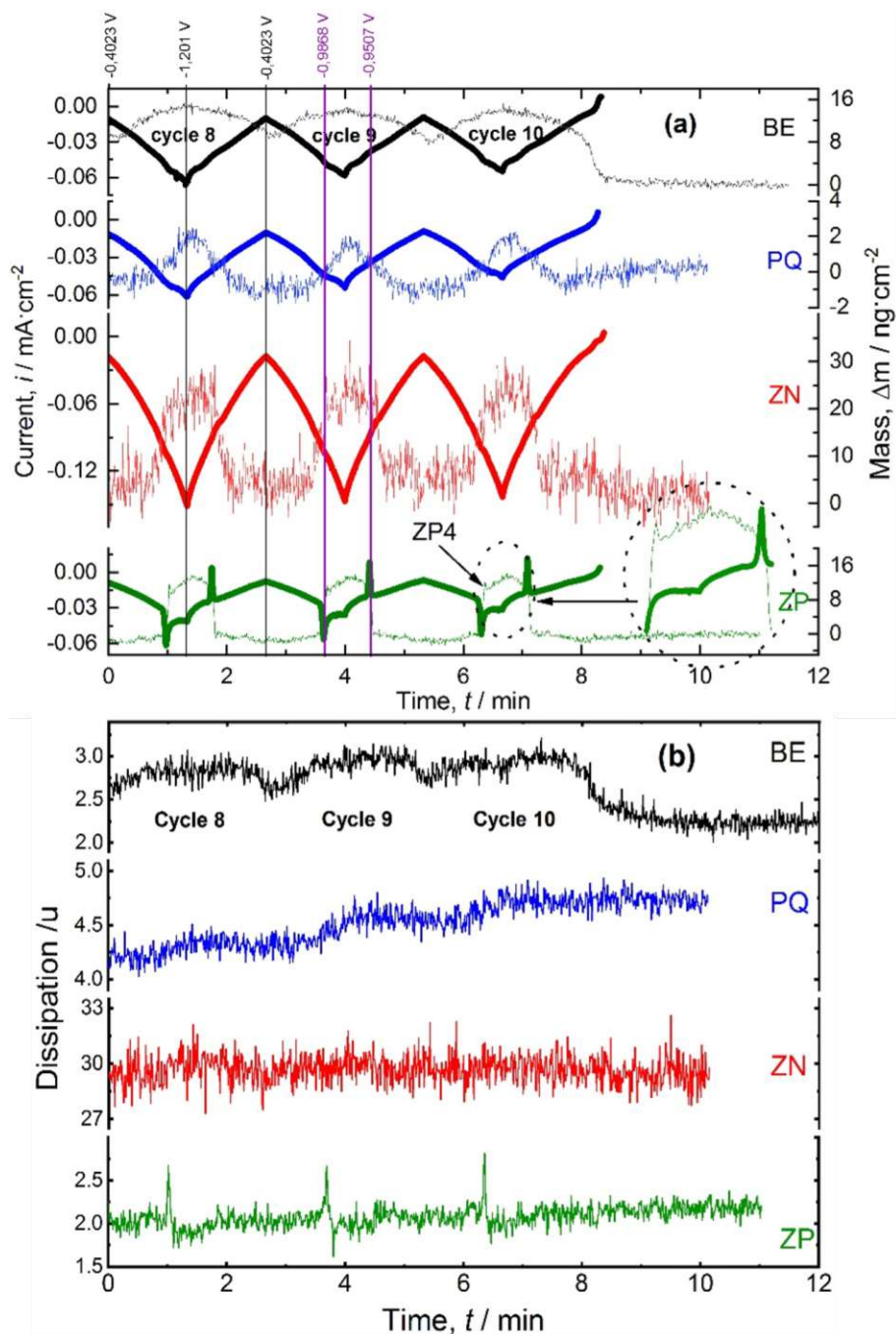
Figure 4.3: Nonreactive cycling (cycling between −0.4 and −1.2 V vs Ag/AgCl). (a) Current and mass against the time for all electrolytes. Thick lines correspond to the current plots; thin lines correspond to the mass plots. (b) Dissipation behavior vs time for all electrolytes. BE: NaOH electrolyte; PQ: 0.1% solution of polyquaternium 2 in NaOH; ZN: zinc electrolyte without polyquaternium 2; ZP: zinc electrolyte with polyquaternium 2. Note for the BE the mass should be treated as indicative rather than quantitative (see the Experimental Section).

region, are observed. This agrees with a compacting of the now depleted polymer. Also, this is in line with the simultaneously measured dissipation. Figure 4.3b shows the dissipation as a function of the time (i.e., applied potential) during repetitive CV cycling within the electrochemical window from −0.4 to −1.2 V. The background electrolyte, the PQ solution, and the neat zincate solution show no particular significant features in the dissipation. All solutions, except the pure zincate solution (ZN), indicate a transient increase of the dissipation within the first few cycles, indicating a surface annealing [73]. Only data for the ZP electrolyte indicate a swift increase, followed by a decrease of the dissipation back to the baseline, upon the initial adsorption of the Zn-loaded polymer. The process occurs over a few points in the QCM-D data, which is recorded every 0.4 s. Each point is therefore 10 times longer in time than the Zimm time, which is calculated as 0.36 ms. The Zimm relaxation time [74] is how long the polymer requires to explore its full configuration space once. Hence, the sharp increase in dissipation occurs over a longer time than the natural fluctuations of the polymer configuration. Figure 4.4 provides another way to visualize this process via a mass vs dissipation plot and the changes happening to the polymer chains at the interface triggered by the potential change. The dissipation and mass increase at the same time (phase 1 in Figure 4.4) as the loaded polymer adsorbs and rapidly undergoes an initial depletion of its load onto the surface.

The depletion is a transient state and dissipation decreases (phase 2) as the polymer stiffens as it reloads with zincate and the surface configuration equilibrates. When the charge is more positive, the zincate (and polymer) is released from the surface, and the mass decreases once more (phase 3). Again this is a strong indication for an initial adsorption, followed by a Zn depletion (due to zincate or zinc adsorption to the metal surface). This effectively modulates the stiffness of the adsorbed polymer, consistent with the observed dissipation fluctuation.

As such we can confirm that the polymer and also the zincate-loaded polymer adsorb at the electrode surface. Effectively, the polymer will hence moderate the deposition at lower potentials from −1.4 to −1.8 V, which is further shown in Figure 4.5. Specifically, Figure 4.5a shows representative results of potentiostatic Zn deposition from ZP and Figure 4.5b from ZN recorded in a QCM-D. At −1.6 V deposition from the ZP solution shows rather limited mass gain and a fast drop
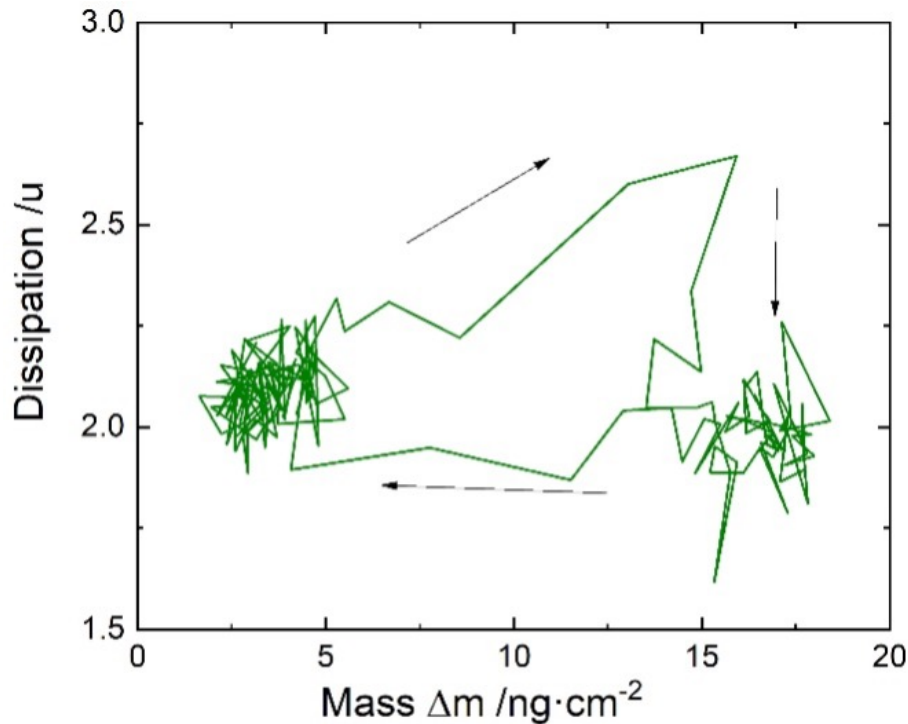
Figure 4.4: Mass vs dissipation plot for one cycle of the QCM-D measurement of the ZP electrolyte shown in Figure 2. The arrows indicate the direction of the cycle with time. The three phases are described in the text.

of the current. Compared to the data for ZN, without the polymer (see Figure 4.5b), the data for ZP at -1.6 V suggest a considerable slowdown of the deposition rate, which is consistent with almost all of the mass deposited deriving from the initial polymer depletion at the interface. Interest- ingly, and as shown in Figure 4.5a, deposition from ZP initiated at -1.8 V indicates a fast initial drop of the deposition rate, followed by a subsequent rise of the rate. This change of the deposition rate also coincides with a significant change of the mass deposition rate (marked by an arrow). The mass gain is initially slow and also much slower in comparison to the rate in the ZN solution (compare rates which are marked by the arrows), which is consistent with an initial and fast depletion of the zincate from the polymer in the ZP solution. The subsequent rise of the current and mass deposition rate clearly suggests a diffusion-controlled deposition following the initial depletion.
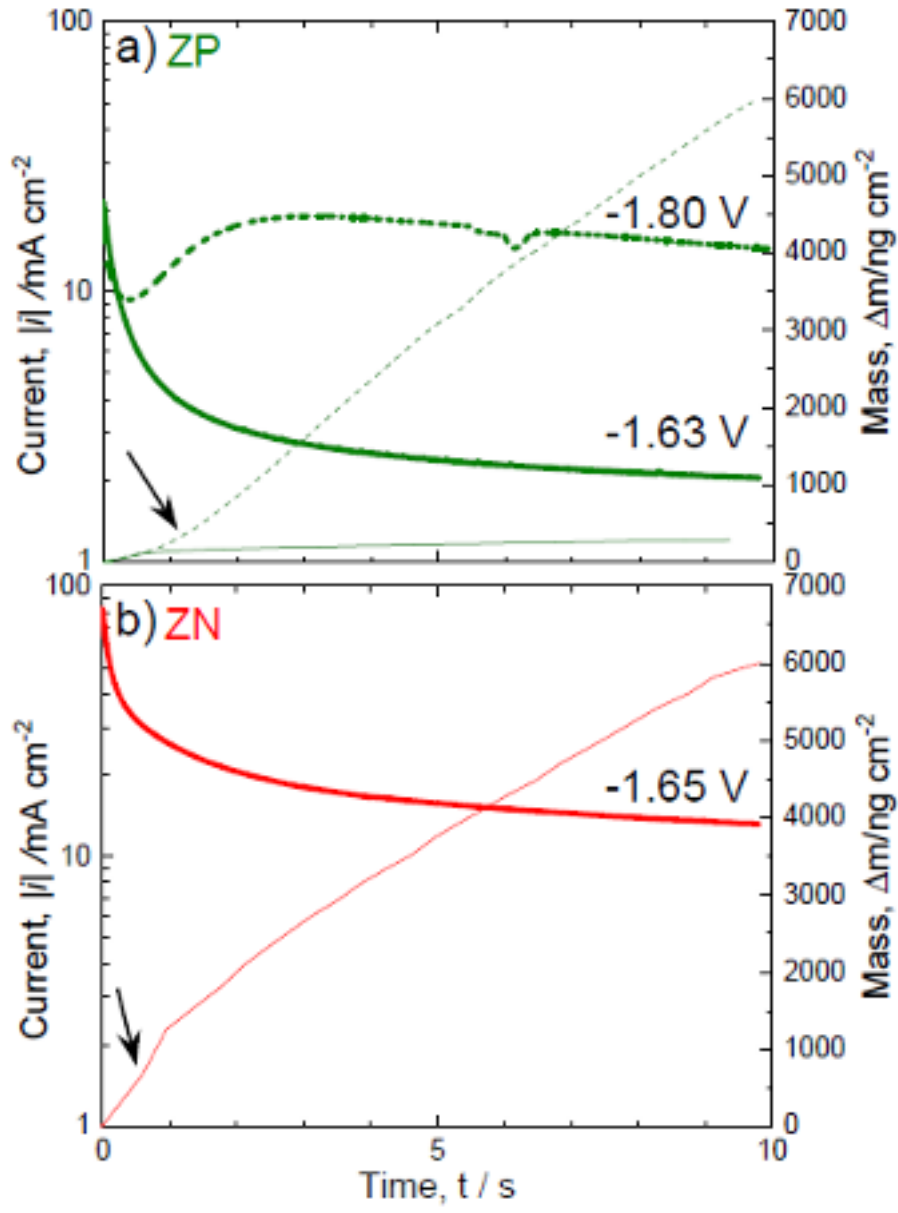
Figure 4.5: Current and mass transient data during potentiostatic Zn deposition from (a) ZP (solid lines at −1.63 V and dashed lines at −1.80 V) and (b) ZN, respectively. Thick lines correspond to the current, and thin lines represent the change in mass.

4.3 Conclusion

A Zn-plating electrolyte contains negatively charged zincate complexes $[Zn(OH)4]^{2-}$ that, in principle, cannot easily approach a negatively charged electrode surface due to electrostatic repulsion. Figure 4.6a shows a schematic of the electric double layer in ZN solution, which mainly consists of sodium co-ions at cathodic potentials where the surface carries a large negative charge, σ. As a result, zincate can only deposit through an outer-sphere reaction. This offers very little to no direct steering and control of the reaction rates.
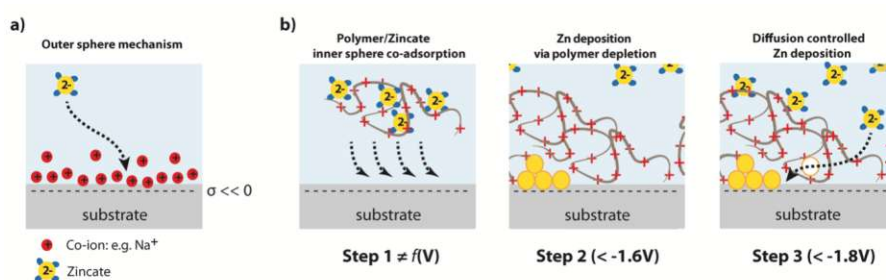
Figure 4.6: Schematic understanding of the PQ-controlled zinc deposition. (a) From ZN solutions the Zn deposition proceeds via an outer-sphere reaction. Because of the high negative surface charge, σ, the inner electric double layer consists mainly of sodium co-ions. (b) In ZP solutions a three-step mechanism proceeds via (1) coadsorption of zincate together with the positively charged polymer, which effectively competes with sodium co-ions in the inner sphere of the electric double layer, (2) during electrodeposition zinc initially deposits via depletion of zincate from the adsorbed polymer, and (3) the depleted polymer subsequently establishes a the layer quality.

As indicated in Figure 4.6b, the PQ polymer coils, on the other hand, are generally positively charged (due to the quaternary amine) and can hence easily approach and adsorb at the gold surface, effectively competing with sodium co-ions in the inner sphere of the electric double layer. Also, PQ can absorb zincate ions forming a zincate loaded and likely still weakly positively charged polymer. This allows the negatively charged zincate to coadsorb to the surface in the inner sphere of the electric double layer. Potential central steps of the mechanism for Zn plating moderated by PQ are also depicted in Figure 6b and can be summarized as follows. In step 1 the zincate/PQ aggregate can easily transport zincate to the surface with a low electrostatic penalty.

Close to the surface, essentially in the inner sphere of the electric double layer, the reduction mechanism described in step 2 can then reduce the zincate ions, while depleting zincate within the adsorbed polymer layer. Yet the polymer film remains at the interface. In step 3 this layer then effectively acts as a moderator of the reduction reaction due to a targeted control of the zincate diffusion through the polymer. Our findings offer interesting insight into how one may tune and control the polymer for making more effective additives for Zn plating and electrodeposition in general.

5 AFM application in the structure characterisation of a zinc layer deposited from an alkaline electrolyte containing a polycationic polymer

The following chapter is a reproduction of my published article that appears in Materials and Corrosion [75]. No additional permission was required as the paper is licensed under a Creative Commons Attribution license CC-BY.

5.1 Introduction

In the first part of this work (see chapter 4) we already investigated the general behaviour and the role of polyquaternium 2 in the cyanide free alkaline zinc bath. The poly quaternary ammonium polymer transports the zincate into the inner sphere of the electrical double layer, where the compound is reduced to metallic zinc. The polymer is adsorbed on the surface and is now free of zincates. Further zincates have to diffuse through the polyquaternium 2 and to be further reduced. We were able to clarify and draw the mechanism of polyquaternium 2 moderated zinc deposition.

In this part, we are going to investigate how polyquaternium 2 acts as an additive in an alkaline, cyanide-free electrolyte. How does the polymer moderate the crystal growth of the electrodeposited layer? To answer this question atomic force microscopy (AFM) was performed to image the deposited zinc layer and so allowed us to visualise the

structure of the layer at the nanoscale. AFM is a technique that can be applied to image surfaces such as metals [76, 77] , ceramics [78, 79], polymers [80, 81] etc. We additionally used low energy ion scattering (LEIS) to understand the composition of the deposited surface and hence further interpret the surface morphology. Thus, one can have a better understanding of the influence of the polymer on the quality of the coating. By performing AFM of a polymer layer on mica, the conformation and role of the polymer in the changes that it causes to the crystal growth mechanism is supported.

5.2 Results and discussion

In this work we used AFM to study the difference between two types of zinc layer. A zinc layer deposited from an electrolyte containing PQ and from one with no polymer additives. This method allows us to image the morphology of the deposited zinc layer. We will discuss the differences between surface images of the variable layers. This will additionally help us understand why PQ enables deposition of a thin, smooth and bright zinc layer.

The imaging reveals some interesting differences. Figure 5.1 illustrates the results of the imaging of the zinc layer deposited at the potential of - 1.48 V vs Ag/AgCl from an alkaline electrolyte containing no additives. At this potential the zinc deposition and the hydrogen evolution reaction (HER) happen simultaneously.[63] It should also be noted that this is an onset of the HER and bulk Zn deposition compared to when polymer additives are included in the electrolyte. All the images in the figure were obtained from the same tip position and are represented as height and phase retrace. We can see in all four images that the zinc layer is composed of a variable grain size. Additionally in Figure 5.1(a) and (b) we can clearly see height variation, that shows that the deposition is uneven. The crystals have different sizes and their shapes are not uniform. The rough surface therefore will not reflect light effectively, as also observed after a significantly longer deposition on the macro-scale in Figure 1.1(a).

Although we have previously proposed a mechanism by which the polymer slows the deposition of zinc,[63] here we were interested specifically in what influence the polymer has on the crystal growth, so that it induces the formation of a smooth and bright layer. In compari-
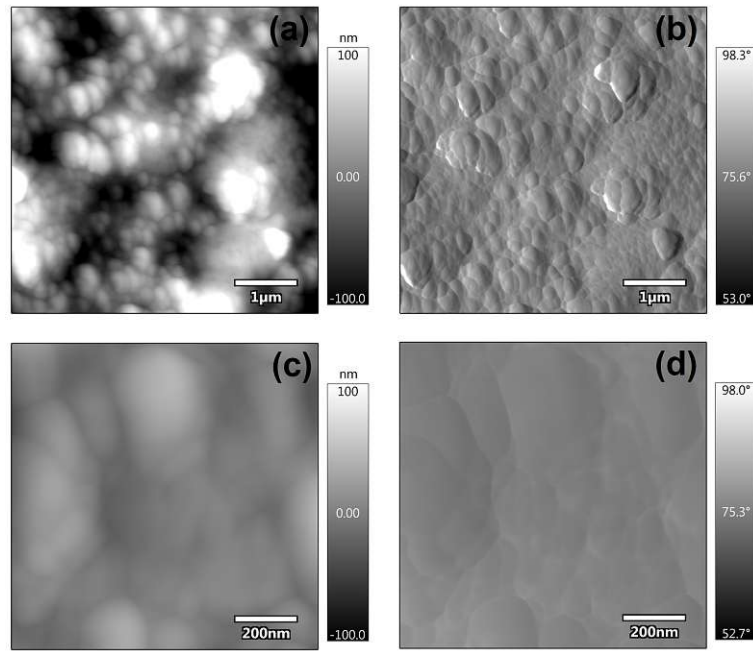
Figure 5.1: AFM images of a zinc layer deposited from an alkaline electrolyte containing no PQ. (a) Height retrace image at 5 micron scan size.(b) Phase retrace image at 5 micron scan size. (c) Height retrace image at 1 micron scan size. (d) Phase retrace image at 1 micron scan size

son to the AFM images of Figure 5.1 deposited without PQ, Figure 5.2 shows the substrate surface after 30 s zinc deposition at -1.43 V vs Ag/AgCl from an alkaline electrolyte containing PQ. At this potential the positively charged polymer coil approaches the surface and the zincate, that is adsorbed within the polymer coil, is deposited, depleting the polymer.[63]

The first observation we make in Figure 5.2(a) and (b), is that, at first glance, the surface does not appear to be completely covered with zinc. This could be explained by the deposition at this potential having only just started. We hypothesise that we may be imaging the first few deposited monolayers of the zinc deposition, particularly in the centre of the image that we image in higher resolution in (c) and (d). We will return to this hypothesis after discussion of the other features observed. In Figure 5.2(b) we additionally see that those crystals, which have started to grow, have a similar oval shape. In the height and phase retraces for the 1 micron image (Figure 5.2(c) and (d)) there is no variation in height. However, there are some small variations in the phase retrace (d), although it is not possible to clearly determine the morphology that they represent. Overall the images in Figure 5.2
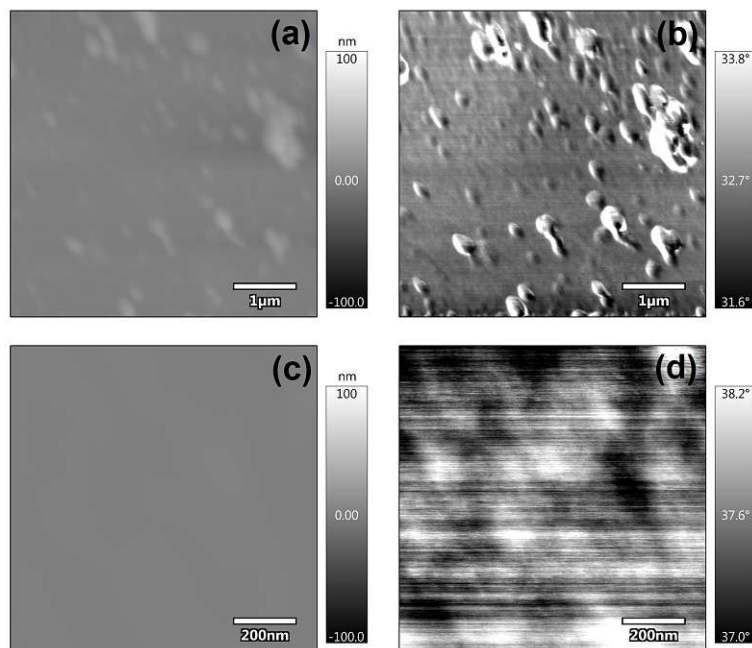
Figure 5.2: AFM images of a zinc layer deposited from an alkaline electrolyte containing PQ at the polymer depletion potential -1.43 V. (a) Height retrace image at 5 micron scan size.(b) Phase retrace image at 5 micron scan size. (c) Height retrace image at 1 micron scan size. (d) Phase retrace image at 1 micron scan size

indicate that when the zincate first deposits from the polymer it is likely that any crystals growing on the surface of the substrate do not follow the same growth mechanism as seen without the polymer in Figure 5.1.

In order to determine whether, as proposed in our above hypothesis, zinc is present across the whole surface even at a deposition potential of -1.43 V, rather than just as islands we performed low energy ion spectroscopy (LEIS). In Figure 5.3(a), the concentration of zinc and gold determined by normalisation to a standard are followed, with each spectrum provided in panel (c). The data points were taken as a sputter depth profile using an Ar^+ ion sputter gun at two different sputtering energies as indicated in the figure. As highlighted in Figure 5.3(b), after the first sputter cycle no gold is recorded but there is zinc present, followed by an increase of both zinc and gold. Although the background intensity of the spectra and other elemental peaks present indicate that the surface is not purely zinc on gold, the data suggest that the zinc is, likely, well distributed across the surface. This is followed by alloying of zinc with the gold through to approximately 4 nm into the top of the gold surface. Here, all other elements (e.g. organic contaminants
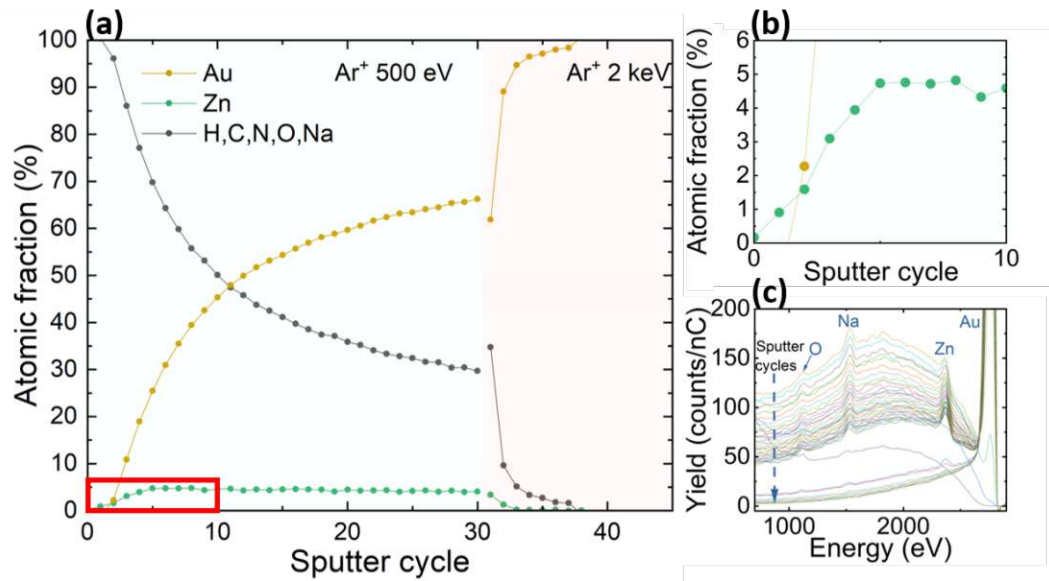
Figure 5.3: Low energy ion scattering results for depth profiles of zinc deposited on gold from the electrolyte containing PQ, taken using an Ar^+ ion sputter gun set at 500 eV (blue shading) and 2 keV (orange shading). In (a) the concentrations have been normalised to pure standards of Zn and Au, where for Ar 500 eV each sputter cycle represents approximately 0.1-0.15 nm of depth into the sample. The red box indicates the area shown in detail in (b). (c) shows the raw spectra for the series of sputter cycles with the contributions from elements other than Au falling away as pure gold is reached after 38 cycles.

and oxygen from oxide formation) are represented by the grey points in the figure. It is interesting to see that there is a significant proportion of other contaminants either present or carried deeper into the surface layer during the LEIS measurement. This is can most likely be explained by the incorporation of the polymer and electrolyte species during the crystal growth or from inter-mixing during sputtering. This intermixing could be varied by the sputter settings and, therefore, is likely to represent the highest possible thickness of the alloyed region. However to fully understand the ion scattering from the surface alloy of zinc and gold accurately would require a more detailed study of the surface components. When combined with modelling of the ion trajectories and any ion induced mixing within the modified crystal lattice, LEIS will be able to further elucidate the full structure of the zinc layer formed on Au.

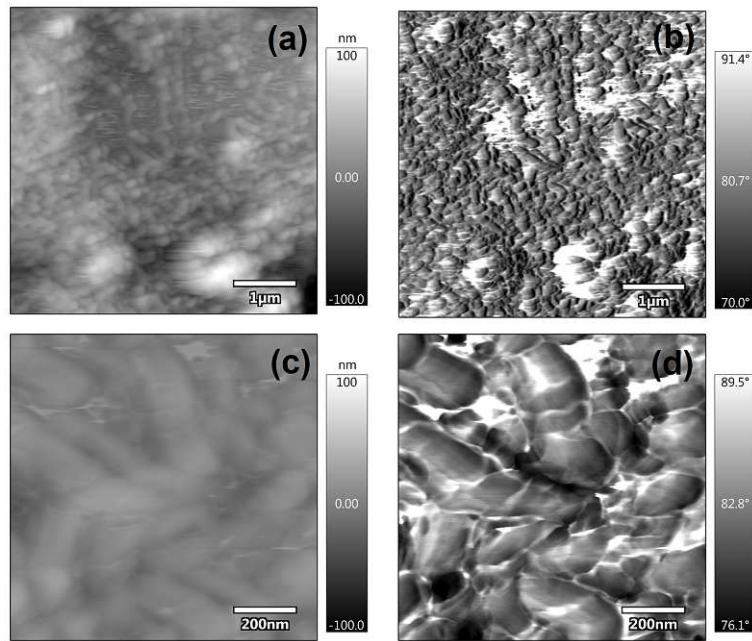Comparing the topography of the zinc in Figure 5.1 (deposited with-

Figure 5.4: AFM images of a zinc layer deposited from an alkaline electrolyte containing PQ for the bulk deposition (-1.56V). (a) Height retrace image at 5 micron scan size.(b) Phase retrace image at 5 micron scan size. (c) Height retrace image at 1 micron scan size. (d) Phase retrace image at 1 micron scan size

out PQ) with the topography in Figure 5.4 (with PQ) shows a huge difference in the structure. Note that Figure 5.4 illustrates the imaging of the zinc layer deposited at -1.56 V vs Ag/AgCl from an alkaline electrolyte containing PQ compared to the potential of -1.43 V that was used in Figure 5.2. Here a diffusion controlled zinc deposition happens as this potential represents the start of the main bulk deposition of Zn.[63] At this lower potential, Figure 5.4(a) shows less height variation than the zinc layer in Figure 5.1(a). This means that the deposition with PQ leads to a smoother and more even layer. Zooming in at the centre of this image shows, as illustrated in Figure 5.4(c) and (d), that the grains have an elongated shape and approximately the same grain size overall. The surface is smooth and well covered. It is clear that when the crystal growth continues with this mechanism and uniformity, the deposition moderated by the polymer, PQ, will also form a smooth, even and bright layer also at the macroscopic level as observed in Figure 1.1.

The way in which the PQ adsorbs at the negatively charged surface and hence directs the crystal growth can be further explored using ex-
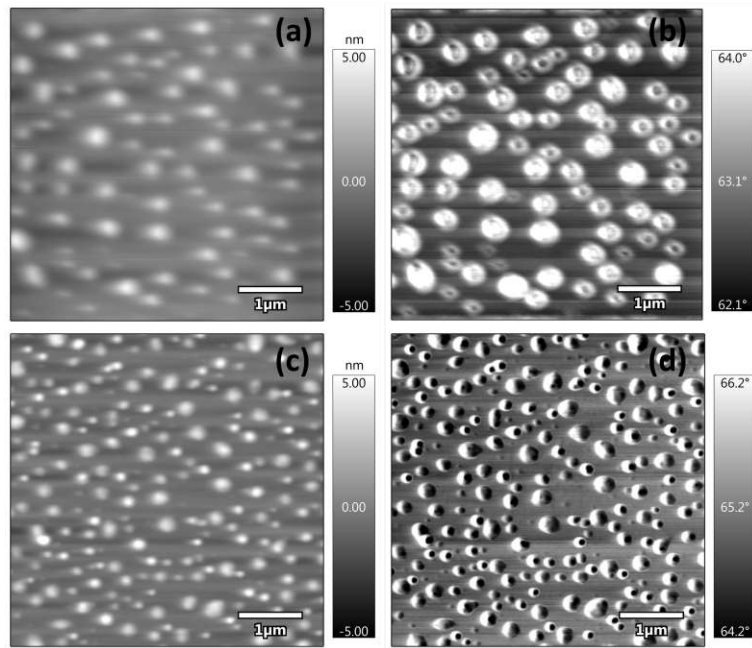
Figure 5.5: AFM images of the adsorbed PQ on mica which was deposited from the zinc electrolyte, rinsed and dried for (a) and (b) 10 mins at 60 °C and (c) and (d) a further 3 days at room temperature. (a) and (c) show the respective height retrace images over a 5 μm scan area and (b) and (d) the phase retrace images.

situ images of the PQ adsorbed to a negatively charged mica surface. This approach has the advantage that the mica does not lose its charge while handling the sample.[82] Figure 5.5 shows circular islands of polymer on the mica surface, which, even after a period of heating, continue to dry out at room temperature and pressure with the radius of the islands continuing to reduce as seen in panels a and c. During repeated imaging these polymer islands could be moved to the edges of the imaging area when the sample was first scanned. However after 3 days of drying the islands remained stable within the imaging area indicating that the polymer mobility on the surface was reduced. The number of islands and volume of polymer also increases with the further drying, which indicates that some of the polymer was spread across the surface outside of the islands. The lower resolution of the islands in the height image compared to the phase images in Figure 5.5b, where they are well defined with a round disc-like shape, could also indicate a covering of polymer across the surface below the islands after the shorter drying period. In Figure 5.6 we further analysed the volume of the polymer islands in a set of AFM images and compared
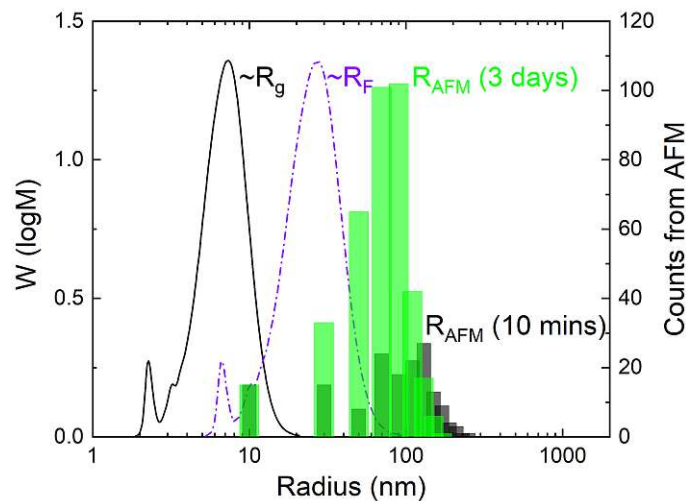
Figure 5.6: Estimated rms radius of gyration R_g for the measured M_W distribution using a freely jointed chain model and an estimated Flory radius using $R_F \approx ln^{3/5}$ in purple for the same distribution in blue. Histograms from the 5um height AFM images of 10 mins drying (black) and 3 days drying (green). PQ was deposited on mica from a basic solution of PQ.

them to the volume distribution that can be estimated for the molecular weight distribution based on the estimated Flory radius, the most likely size characteristic when the polymer is in a good solvent, using $R_F \approx ln^{3/5}$, as well as for the R_g, which is the more likely characteristic size when dehydrated. The comparison of the size distributions indicates that there is more than one chain in each of the islands and therefore, in hydrated conditions, the polymer is most likely adsorbed more densely than a single monolayer of polymer. Therefore the diffusion barrier, which the polymer expands and spreads across the surface to form in the hydrated (electrolyte) conditions, is expected to provide a good coverage of the surface. The zincate retained within the initially adsorbed PQ will also be well distributed across the surface enabling the initial depletion of the polymer to deliver the zinc everywhere.
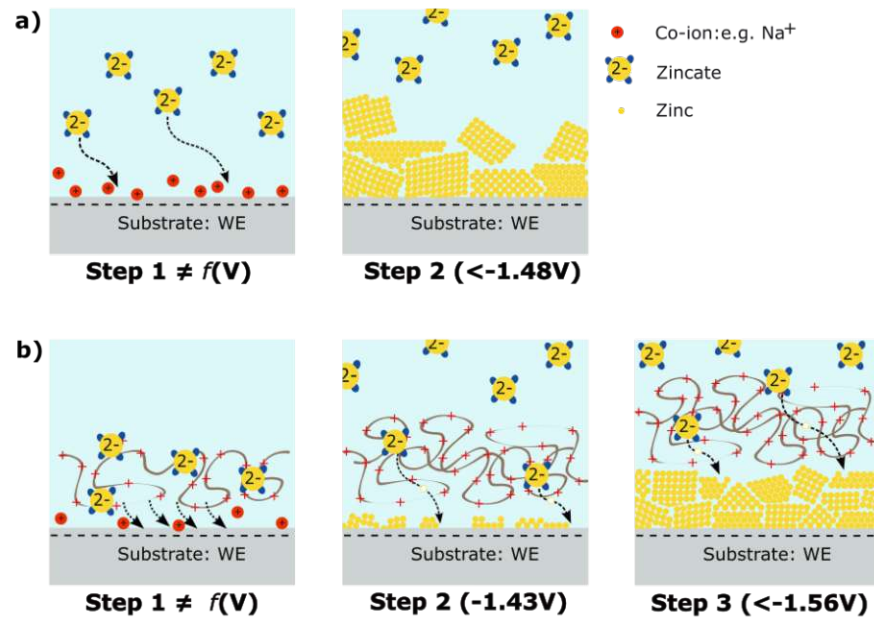
Figure 5.7: Model sketch illustrating the zinc deposition in: a) an electrolyte containing no polymer and b) an electrolyte containing PQ.

Figure 5.7 illustrates the proposed growth mechanism in more detail with the schematic of a non controlled (Figure 5.7a)) and a polymer controlled zinc layer deposition (Figure 5.7b)). When there is no polymer present, Figure 5.7a), we propose that the crystal growth follows a Volmer-Weber type, island growth mechanism. Multiple nucleation sites are established on the surface. However, the further crystal growth continues on top of those initial nucleation sites inducing the growth of an island. The incorporation of the atoms does not happen uniformly and causes the crystal grains to grow unevenly. They also appear to form new nucleation sites on top of the islands leading to crystals that are inherently weakly bound to the surface.

However, when a polymer additive, PQ, is included in the electrolyte the crystal grain morphology observed in the AFM images indicate that the mechanism is different. We therefore propose that it proceeds as follows. In step 1 of Figure 5.7(b), the zincate uses the polymer to approach the surface through the inner layer of the electric double layer. As soon as the potential of -1.43 V is reached the polymer is depleted of zinc and the reduction of zinc onto the surface starts as shown in step 2 of Figure 5.7(b). The first layer or layers of zinc appears to completely

cover the surface with perhaps some islands on top. This is supported by both the AFM images in Figure 5.2and the LEIS data presented in Figure 5.3, which indicates that there is zinc at the surface of the gold through to approximately 4 nm into the top of the gold surface.

In step 3 when the potential for bulk deposition, -1.56 V, has been reached, we see that the surface is completely covered. In contrast to the case where there is no polymer, the grains size is smaller. The crystallites are also smoother and more evenly distributed across the surface. This suggests that the growth mode has changed from the Volmer-Weber type island growth mechanism to a more layer-by-layer dominated Stranski-Krastanov type crystal growth mechanism. The fact that the polymer inhibits the deposition and creates a diffusion barrier to the zinc reduction reaction, appears to give time to the zincate to minimise its energy within the growing crystal structures at the surface and thus find a suitable place to deposit. Hence smooth, small, more uniform crystallites are formed compared to the deposition without PQ.

5.3 Conclusion

It is well known that polymer additives play an important role in forming smooth, visually appealing, shiny zinc layers during electrodeposition. We have previously established that, with the zincate and the substrate surface both negatively charged, the deposition must happen through an outer-sphere reaction.[63] Here we have explored the deposition and growth mechanism during electroplating of zinc from an alkaline zincate electrolyte. Deposition of zinc without a polymer additive led to a rough and dull layer. Including the polymer additive, PQ, improves the appearance of the deposited metallic layer, to be thin, shiny and smooth. The growth mechanism of the zinc crystallites at the model gold surface appears to be governed by the electrostatic charges present at the surface. When there is nothing to slow the reduction of zincate to zinc at the surface an island (Volmer-Weber type) growth mechanism dominates. The polymer, PQ, appears to wet the negatively charged surface well, as also indicated in the dried images of PQ on a negatively charged mica surface, it therefore creates a diffusion barrier across the whole surface. Once the positively charged polymer is present to overscreen the charge at the surface, the mecha-

nism appears to change to a layer-by-layer dominated crystal growth mechanism. This leads to smooth, more uniformly sized crystallites.

Our further understanding of the growth mechanism of electrochemically deposited zinc can be used to improve deposition in industrially relevant conditions. It is clearly the diffusion through the polymer layer at different charge/potential values that dictates the appearance of the zinc layer and the rate at which the deposition takes place. Therefore improvements to additives need to take the polymer structure and charge characteristics into consideration. Changes such as increasing flexibility and the positive charge in the main chain of the polymer can help improve the electrodeposition of zinc. In addition to that, the molecular mass also plays a major role.

6 Polymer synthesis and comparison with the commercially available polymer

6.1 Introduction

Polyquaternary ammonium polymers are compounds that have been used in hair products for a long time. [83] Since a few years they have become very famous in the electroplating industry. [84–86] It has been found that small amounts of them in electrolyte improve metal deposition. There are different ways to produce polyquaternary ammonium polymers.[84, 85, 87] But the most commonly used method is a condensation reaction between urea and an amine and a subsequent polyaddition reaction with a dihalogenide compound. In a condensation reaction, two molecules are linked together and small low molecular weight compounds (water, hydrogen chlorides, alcohols, etc...) are split off. A polyaddition is a polymerisation reaction in which monomers are linked together to form a macromolecule. The polymer is formed through individual independent addition reactions between functional group of molecules with low degrees of polymerisation such as dimers, trimers, oligomers. The Activation energy is approximately the same for each reaction step regardless of chain length. The polymer is form at nearly completed reaction. The starting compounds must have at least two functional groups. To achieve a high degree of polymerisation X_n the amount of monomers used should be stoichiometrically matched to the reaction equation. High degrees of polymerization and thus high molecular weight are only achieved at very high conversions. The degree of polymerization of step growth reactions is strongly conversion dependent. The correlation between

degree of polymerization and monomer conversion p can be determined mathematically using the Carothers equation in (6.1).[88, 89] For a reaction of the type:

$$A\text{——}A \ + \ B\text{——}B \ \longrightarrow \ \left(\text{——}A\text{——}AB\text{——}B\text{——}\right)_n$$
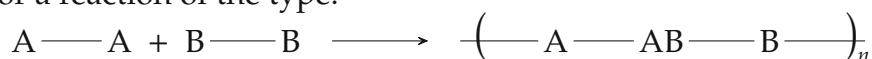
The Carothers equation is describe as follow:

$$X_n = \frac{1+r}{1+r-2rp} \tag{6.1}$$

With

$$r = \frac{N_A}{N_B} \tag{6.2}$$

X_n = degree of polymerization

p = conversion

r = ratio of number of functional group such that it is ≤ 1

N_A = number of functional group A

N_B = number of functional group B

Knowing that the degree of polymerisation is define as the quotient of average molecular weight M_W of the polymer and the molecular weight of the repeating unit M, the Carothers equation can be use to develop a polymer with a specific molecular weight.

$$X_n = \frac{M_W}{M} \tag{6.3}$$

The Carothers equation can be applied to 3 different step growth reactions. The linear A-B systems, the linear A-A/B-B systems and the non-linear step growth reactions. This work is about a linear A-A/B-B system. Both monomers carry one of the functional groups at each end. The relationship of the Carothers equation described in equation (6.1) is adapted for our system. Polymers with large molar mass seem to be effective for our target. In order to obtain an average molar mass in the same range as that of polyquaternium 2, we need to use an equimolar amount of monomers. Thus, the Carothers equation is now described as follows:

$$X_n = \frac{1}{1-p} \tag{6.4}$$

One important aspect of this synthesis was to avoid carcinogenic and mutagenic substances during the preparation. In some cases, residual

monomers remain in the finished product. This can complicate the use of the product in industry. Because nowadays the use of toxic products is more and more restricted. The aim of this synthesis was to produce a polymer that performs better in alkaline zinc baths than conventional commercial products.

6.2 Synthesis

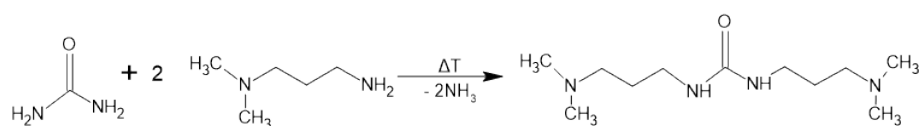### 6.2.1 Synthesis of the intermediate: 1,3-bis[3-(dimethylamino)propyl]urea

Figure 6.1: Condensation reaction for the formation of the intermediate compound: 1,3-bis[3-(dimethylamino)propyl]urea

1.5mol urea and 3mol N,N-dimethylaminopropylamine were weighed into a 3-neck flask equipped with a magnetic stirrer, a reflux condenser and a thermometer. The flask was then heated for a total of 16h at 160°C. Samples were taken from the main batch after certain times (after 3h, 5h, 7h, 11h and 16h) and named differently (sample A (3h), sample B (5h), sample C (7h), sample D (11h), sample E (16h)). From a temperature of approx. 145°C ammonia is split off (strong ammoniacal odour). The longer the heating time, the darker the sample became.

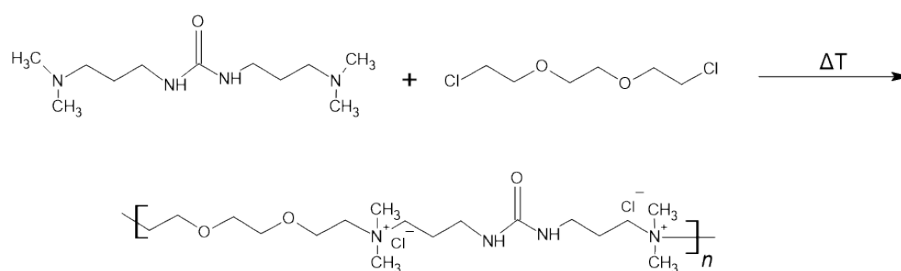### 6.2.2 Synthesis of the poly quaternary ammonium polymer

Figure 6.2: Polymerisation reaction of 1,3-bis[3-(dimethylamino)-propyl]urea with 1,2-bis(2-chloroethoxy)ethane

0.1mol of the intermediate (sample A, B, C,D or E) was weighed into a 3-neck flask equipped with a magnetic stirrer, a reflux condenser and a thermometer and heated to 100°C. Then 0.08mol of 1,2-bis(2-chloro-ethoxy)ethane was added slowly. The mixture was then stirred until the mass was almost solid. Then 50g of water was added to dissolve the mass. The colour of the final product depend on the colour of the intermediate. The best performer during the zinc deposition in a Hull cell was the polymer made with the intermediate Sample E (Sample name is Sample E1). That why we will only talk about sample E1 in this chapter.
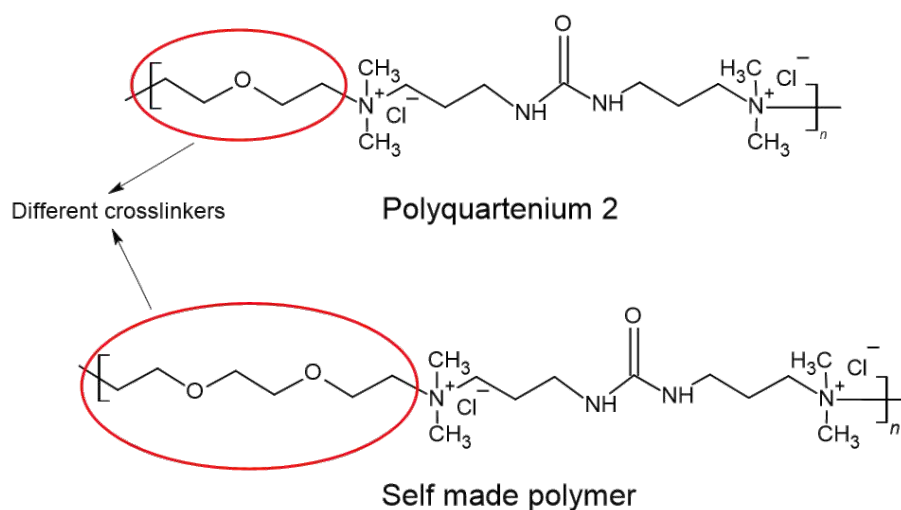
6.3 Comparison

Figure 6.3: Structure comparison between polyquaternium 2 and the self made polymer

The synthesis of a polymer that can positively moderate the zinc deposition in a alkaline electrolyte was successful. The difference with the commercial polymer is the crosslinker. We used 1,2-bis(2-chloro-ethoxy)ethane rather than bis(2-chloroethyl)ether. And thus added a little more flexibility to the backbone chain. You can also vary other parameters in the polymer to achieve better results than with polyquaternium 2. For example, you can vary the chain length, the crosslinker, the side chain. So after using the sample E1 as additive in the electrolyte to deposit zinc on a steel shit, the layer thickness was measured. Now we will compare the optical characteristic of the sheets, the layer thickness distribution and the molecular weight distribution to see which

between the commercial and the self made polymer is the best performer. First of all it was important to do the GPC analysis to confirm the formation of a polymer during the synthesis. Figure 6.4 show the molecular weight distribution for both: a) the polyquaternium 2 (commercial product) and b) sample E1. Figure 6.4 b) confirm that sample E1 is actually a polymer. The molecular weight distribution looks different from the one in Figure 6.4 a). They are more low-molecular compounds in Sample E1 than in Polyquaternium 2. The peaks at about 2500 Da, 4500 Da and 7000 Da in 6.4 b) show that they are more molecules with a molecular weight smaller than the average molecular weight. The average molecular weight is 20000 Da for the polyquaternium 2 and 15000 Da for sample E1. The fact that sample E1 has a lower molecular weight means that the polymerisation reaction wasn't completed. Then normally for an equimolar amount of monomer the conversion should be close to 99%. This probably means that the reaction was stop earlier than needed. At this stage we tried to separate the low molecular compound with a dialysis (ultrafiltration) treatment. But it wasn't successful. The method or the membrane used for the separation was probably not suitable to this polymer solution.

The Hull cell experiment showed that both polymer produce a nice thin, smooth and shiny zinc layer which is represented in Figure 6.5. This figure shows the pictures of zinc coated steel sheets using as bath additive: a) Polyquaternium 2 (commercial product) and b) Sample E1.

During both experiments, hydrogen evolution was clearly visible at the working electrode. However, the hydrogen evolution was much stronger when using the self made polymer. There was also much more foam created in the cell than when using polyquaternium 2. In addition, the colour of the electrolyte changed from slightly yellowish to purple. These differences compared to the bath with polyquaternium 2 are most likely due to impurities and small molecular compounds in the polymer solution. The laboratory polymer could not yet be properly purified. Electrochemistry experiments, specially cyclic voltammetry experiments induce the cyclic voltammograms that are represented in Figure 6.6. Even here both sample are very similar. Both CVs schow the diffusion controlled deposition of zinc. But the slope of the deposition peaks of sample E1 shows that the diffusion through the adsorbed polymer is slower. An other interesting aspect of those CVs is that

Die approbierte gedruckte Originalversion dieser Dissertation ist an der TU Wien Bibliothek verfügbar.
The approved original version of this doctoral thesis is available in print at TU Wien Bibliothek.

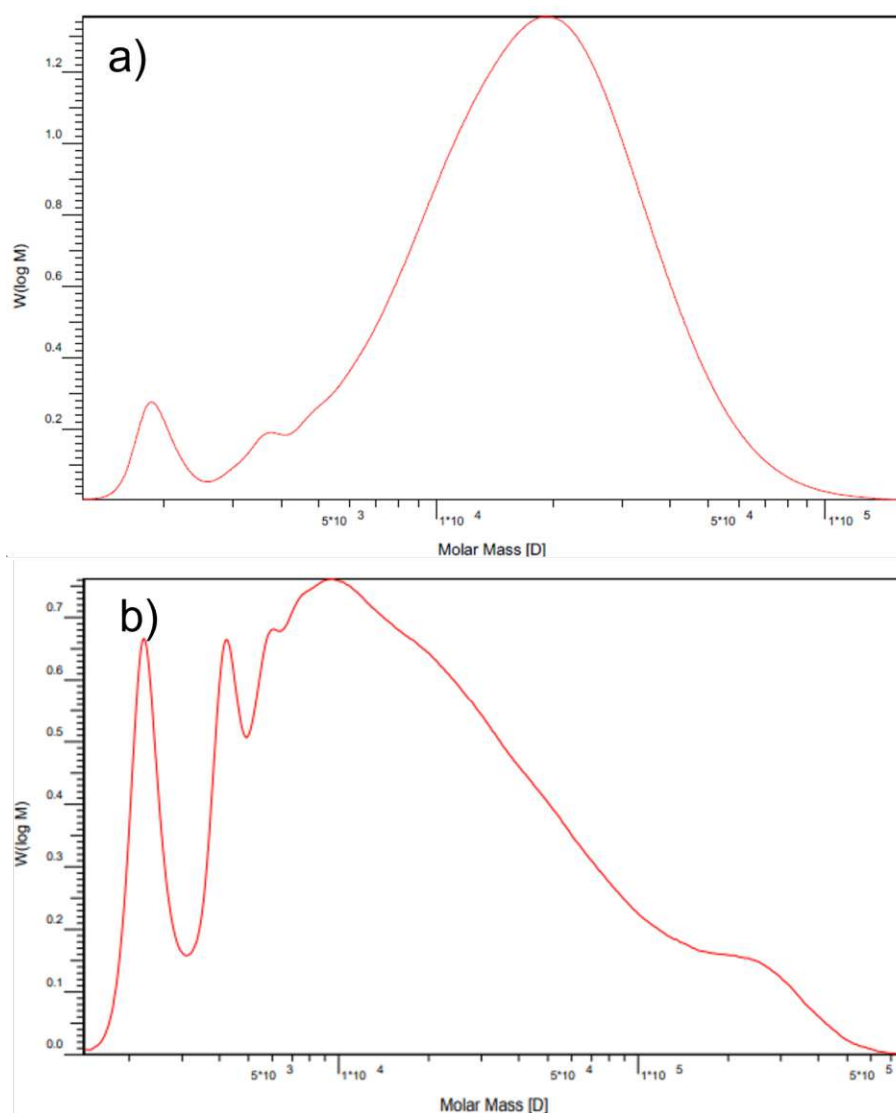TU Bibliothek
Your knowledge hub
WIEN

Figure 6.4: Molecular weight distribution of: a) polyquaternium 2 and
b) self synthesized polymer sample E1

current yield is lower in sample E1 than in polyquaternium 2. This is
in accordance with the fact that the barrier effect of sample E1 to zinc
ions is stronger than polyquaternium 2. We see furthermore that all
peaks in sample E1 are shifted to more negative potential.

Figure 6.7 represents the Layer thickness distribution on zinc coated
steel sheet from an alkaline electrolyte containing the commercial poly-
mer (Black plot) and the self made polymer (red plot). When we
compare both plots we first observe that thickness distribution for the
polyquaternium 2 is steeper than for sample E1. In general the layer
thickness distribution on the sheet with polyquaternium 2 is higher
than with sample E1. The thickness varies between 6.2 μm and 4 μm
for polyquaternium 2, while it varies between 4.6 μm and 3.2 μm for
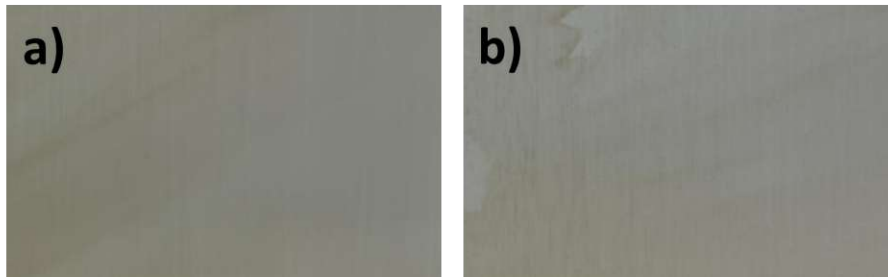
Figure 6.5: Pictures of zinc coated steel sheets from an alkaline plating bath containing: a) polyquaternium 2 and b) self synthesised polymer sample E1

sample E1. Sample E1 inhibits the reaction in high and low current density more than the commercially available product polyquaternium 2. The sample E1 is a mixture of high and low molecular weight compound. This may explain why sample E1 controls the deposition in high and low current density. This probably means that low molecular weight cationic compounds inhibits more in the low current density site while high molecular cationic compounds rather inhibits in the high current density site. Looking at the layer thickness distribution shows that sample E1 performs better than polyquaternium 2.

6.4 Conclusion

The purpose of this was first of all to understand the behaviour of polyquaternium 2 in a alkaline zincate electrolyte during the zinc deposition and on the other hand been able to synthesise a polymer additive that works at least as good as polyquaternium 2. Understanding the behaviour of this polymer help us creating a other polymer additive that also influence the zinc deposition in a good way. We saw in the molecular weight distribution that the synthesis was successful. Comparing the layer thickness distribution also showed that from both polymer sample E1 was the best performer. It inhibits stronger than Polyquaternium 2 in high and low current density. This is probably due to the fact that sample E1 contains more low molecular weight compounds than polyquaternium 2. For further experiment we should probably synthesize low molecular weight cationic compounds to be able to confirm this idea. To reduce the molecular weight of a compound during a polyaddition reaction we need to reduce the mole amount of one of the starter compound or rather add a monofunctional compound to the
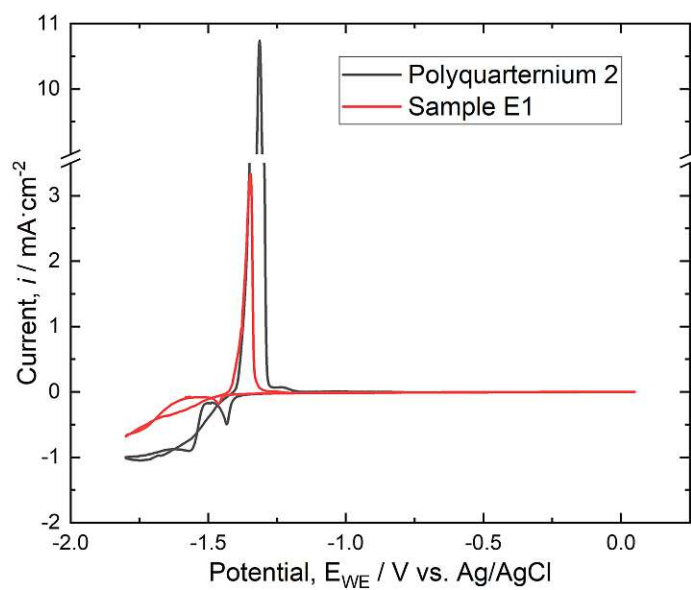
Figure 6.6: Cyclic voltammograms of the cyanide free alkaline zinc electrolyte containing sample E1 (red line) and polyquaternium 2 (black line)

reaction. This is theoretically verified by the carothers equation (6.1).
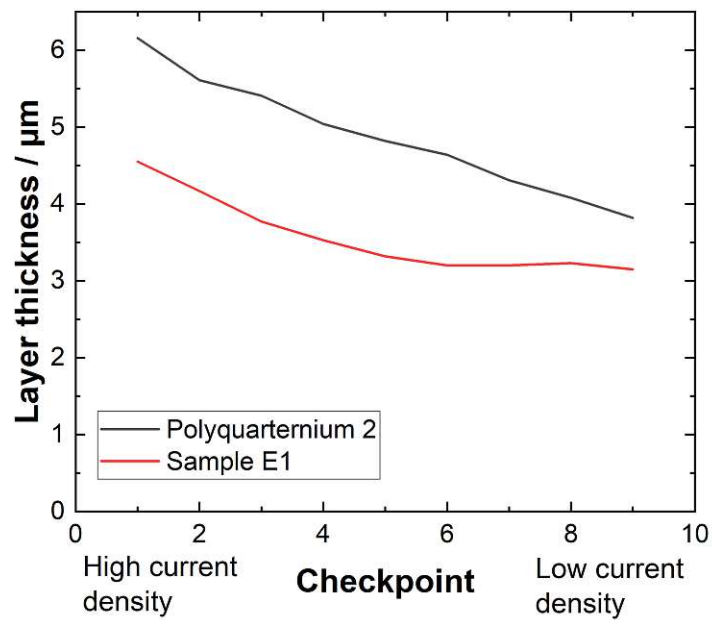
7 Development of a method to measure the layer thickness in real time using laser interferometry

7.1 Introduction

It has always been clear that interfacial reactions are very important for metal deposition. This is the only way to understand how the additives within the electrolyte influence the deposition process. A good zinc coating deposition therefore definitely depends on the composition (organic and inorganic components) of the electrolyte, the temperature, the current density, the bath voltage etc... In industry, zinc baths are used several times and thus additives can be consumed and, in addition, impurities of an organic, inorganic or metallic nature accumulate in the electrolyte. The concentration of the components of the electrolyte must vary within certain limits in order to deposit an optimal layer. The concentration of the impurities must also be monitored because the layer properties deteriorate above a certain concentration. Dirty electrolytes cause rough and poorly polishable coatings with poor corrosion protection. Atomic absorption spectrometry is mostly used to monitor the concentration of metallic impurities. However, this is not enough to eliminate the occurrence of a defect. In practice, it is recommended to perform a check with the Hull cell (See Chapter 1. This way, one can ensure, that there is still enough brighteners available to enable the deposition of a bright metallic layer. For this purpose in the industry the pay attention to the optical appearance of the Hull-cell after deposition. A matt finish for example is an evidence for a deficit of brighteners. But to determine the real concentration of brighteners in electrolytes they mostly use titration. To ensure the

quality of the deposited layer, small amounts of the electroplating bath are needed for Hull cell testing [90].

Thanks to the Hull cell, the quality of the coating can be followed using the test sheet over a specific and adjustable current density range. The test sheet is well defined in the Chapter 3. This is of course possible due to the special construction of the Hull cell, in which the anode and the cathode are not arranged parallel, but angular to each other. This creates different distances between the anode and the cathode, so that the deposition at the cathode (working electrode) takes place with decreasing current density from left to right. Figure 7.1 shows how counter and working electrodes are placed in the hull cell, in order to create the current density difference along the cathode. The electrochemical deposition of the zinc is thus examined over a wide current density range.
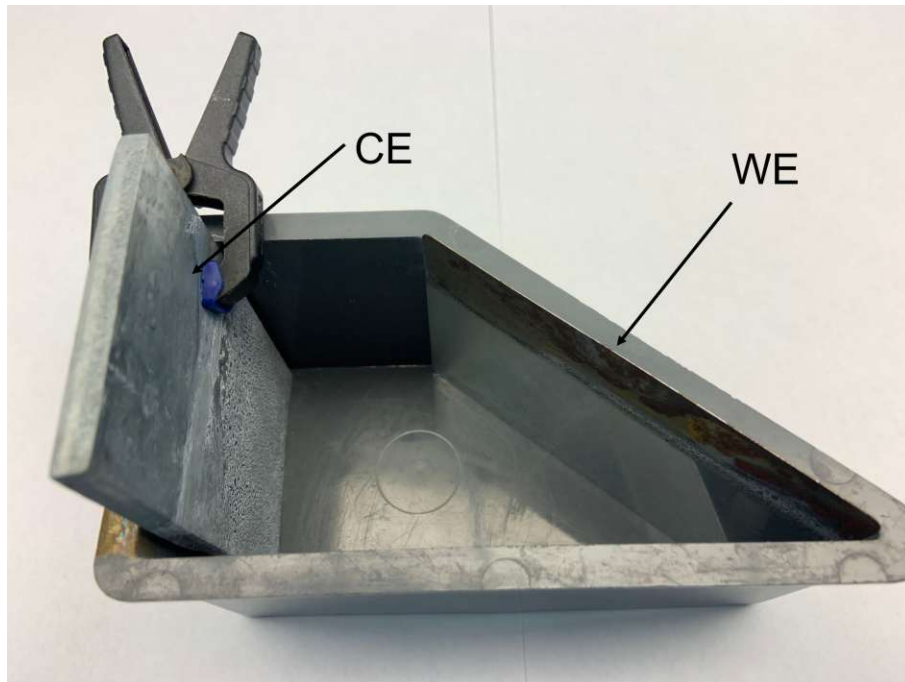

Figure 7.1: Hull cell showing the anode (counter electrode, CE) and the cathode (working electrode, WE)

Until now, the quality of the electrolyte has normally been assessed by the visual appearance of the test sheet, by the adhesion and ductility of the deposited layer and finally by the layer thickness distribution over the entire sheet. For this project, the measurement of the thickness of metal layers is the focus of our interest.

Nowadays there are different methods to measure the thickness of deposited layers. There are non destructive methods such as elec-

tron probe microanalysis, X-ray fluorescence, ellipsometry, Rutherford backscattering spectroscopy etc... and also destructive methods such as secondary ion mass spectrometry, mechanical cross-sectioning, ion beam cross-sectioning, atomic absorption spectroscopy (AAS), inductively coupled plasma mass spectrometry (ICP-MS) etc... [91–93]

For our project, we had to think about the applicability or adaptation of these methods to our basic idea. We had to check which method could be best adapted to a Hull cell. For this we had to see how the methods work individually, what advantages and disadvantages they have. In any case, the measurement method had to be usable for an in-situ layer thickness measurement.

First we describe the destructive methods that can be used for the metal layer thickness measurement. There is mechanical cross-sectioning [92, 94–96], which consists of three steps: The sample preparation, the microscopic analysis and the data processing. For the measurement, the sample is cut in half and observed cross-sectionally with optical or scanning electron microscopy to determine the layer thickness. The sample preparation is very time-consuming and consists of cutting the sample, embedding and polishing the section. Here you have to pay attention not only to the blade of the cutting machine, but also to the speed of the cutting. Because the layer can be damaged due to the heat and can then be detached. Embedding the sample consists of protecting the layer of interest while covering the sample with a resin before cutting. After cutting the whole sample is covered with the resin except the section, where the layer is going to be measured. Polishing the sample near to the section is necessary to eliminate residue caused by the peeling off of the less adhered coating. To be able to have information about the layer thickness we need to transversely examine the cross-section with the optical or the electron microscope. Using optical microscopy makes sense when there is a high contrast between the different layers. The distance between two different layers is defined by the Abbe principle and should be bigger than 1 micron for the layer to be measured. For layer thicknesses smaller than 1 micron and for less contrast between the layers scanning electron microscopy is more appropriate. Electron microscopy is not only expensive, but it can also only be used for conductive materials. Furthermore, the sample to be measured must be resistant to high vacuum and electron beam. However, there is no need to be concerned about this if working

with metallic layers.

In contrast to mechanical cross-sectioning, ion beam-sectioning [92, 97] is fast in its application. A maximum of 60 min is enough to complete the profile characterisation of a sample. This method consists of creating trenches on a layer by rastering of the sample surface with focused ion beams. The sputtering effect of the ion beams permits in-depth observation of the sample. Destructive methods also include the Calo Tester [92, 98]. In this method, the sample is fixed on a holder with adjustable angle. A steel sphere covered with an abrasive substance is placed on the sample. It is important to ensure that the ball is also in contact with a rotating cylinder. Since the cylinder causes the ball to move. Depending on the hardness of the sample and the angle adjustment, a circular crater is formed, which reveals the different layers within a few minutes. Just as with cross-section methods, the different layers are distinguished from each other only if they have different colours. In comparison with cross-section methods the Calo Tester analysis is faster and additionally the sample destruction is local.

There are also non destructive methods [92, 99, 100], which can be used for the layer thickness measurement of metallic layers. The most widely used analysis method is X-ray fluorescence spectroscopy, because it's fast, easy to use and non-destructive. Atoms in the layer are ionised when they come in contact with high energy X-rays and are excited. During the relaxation process, characteristic fluorescent photons are emitted, which are collected by a detector and finally analysed. Interferometric methods such as white light scanning interferometry and multi-wavelength interferometry are used to measure the thickness of metallic and polymer layers without destroying them [99, 100]. Interferometry [101, 102] is a measurement method that uses the phenomenon of interference of waves in the form of light, radio or sound waves. One speaks of white-light interferometry when the interference effects, that occur when the light (with multiple wavelengths in the visible part of the spectrum) reflected from the measurement object is superimposed on the light backscattered by a high-precision reference mirror, are used. This allows the height profile of a sample to be determined. The principle here is based on the way Michelson interferometers work. Light is shone on a semi-transparent mirror and thus split into two beams. While one beam hits the object, the other is reflected by a reference mirror. The transmission at the mirror causes

both beams to come together again and interfere. If the examined object is moved in the z-direction or if a layer is deposited on the object, the amplitude of the interference signal changes depending on the path length difference of the two beam components. The result is an interferogram. The distance between the maxima or rather the minima in the interference pattern is half the wavelength of the light used, since the path difference between the two interferometer arms is passed through twice. If a certain position has been set as the zero point in advance, the actual height of the sample can be determined from this. If the sample surface is shifted by a certain distance, the entire interferogram on the z-axis is shifted by this value.

After looking at all the methods available for determining the thickness of a metal layer, it became clear that interferometry would be best suited to our project. With destructive methods, the layer to be measured is destroyed and then analysed to determine the layer thickness. For this, the layer must already be completely built in order to destroy it afterwards. Therefore, these methods unfortunately cannot be used for a layer thickness measurement in real time. In contrast to the destructive methods, the non-destructive methods can be used for an in situ layer thickness determination. The adaptation of the methods to an electrolytic metal film deposition is difficult but not impossible due to their experiment setup. For this project it was imperative that the analysis take place without contact with the working electrode in order to not disturb the field lines during the deposition process. It was also important that the method is fast enough, as we needed to determine the thickness in real time. This means that there is no time to, for example, prepare the sample or cut it. So, due to the feasibility, we decided to use laser interferometry.

The setup is easy to realise with the laser head that can be flexibly fixed to illuminate the sample. Here we used a laser sensor head from the company Attocube systems AG (See specifications in Chapter 3. The interferometer emits a monochromatic laser beam, a small part of the beam is reflected within the sensor head and forms the reference beam. The remaining laser light is directed at the object to be measured. There it is reflected and thus returns to the sensor head and the control unit. The reference beam and the reflected beam interfere with each other and, depending on the distance of the measuring object, generate a more or less strong signal at the photodetector of the device. If the

distance is large, the signal will be large. In our case when we deposit zinc, the distance between the target and the laser is reduced. That means the signal is also reduced. So in this way we can measure the layer thickness [103]. This new type of frequency analysis of the signal was developed by the company attocube systems AG and can be used to determine the change in position of the target. The idea is to use this technique at some point in the future to potentially create either a direct in situ monitoring on suitable components being plated or an in line version of a Hull cell testing. The aim of this work is to develop a method of measuring the thickness of the metallic (zinc) layer in real time while the deposition reaction is still happening.

7.2 Experimental

The electrolyte solution was prepared in the same way as the solution used in Hull cell experiments. To prepare the zincate electrolyte, zinc oxide is dissolved in a highly concentrated NaOH solution. The concentration of the zinc ions in the zincate electrolyte is 0.29 mol/l and that of the NaOH is 3.8 mol/l. The final electrolyte use for the experiment was then prepared by mixing 200ml of a zincate solution with 7.5ml of base solution and then diluted to 250ml with water. The base solution for this experiment consists of three components. For a 50 ml solution, 2.25 g (active ingredient content) polyquaternium 2 was mixed with 3.25 g Lugalvan G35 and filled up to 50 ml with water.

The working electrode (iron sheet) was hung in a plastic container (lid of a plastic jar) and the counter electrode was fixed next to it in order to create a current density gradient, as in the Hull cell (see the experimental setup in Figure 7.2). Next the electrolyte solution was added so that the working electrode was only covered by a thin layer of electrolyte. At this point it is really important to not use to much electrolyte to be able to be successful with the experiment. The depth of the amount of electrolyte covering the working electrode is approximately 1 mm.

The laser head was hung above the working electrode. After switching on the laser, the laser beam was aligned uniformly and finally the power supply for the deposition current was switched on. The zinc layer was deposited at 1 A and 4 V for 15 min. During the deposition the laser measured the distance between the target (working electrode)
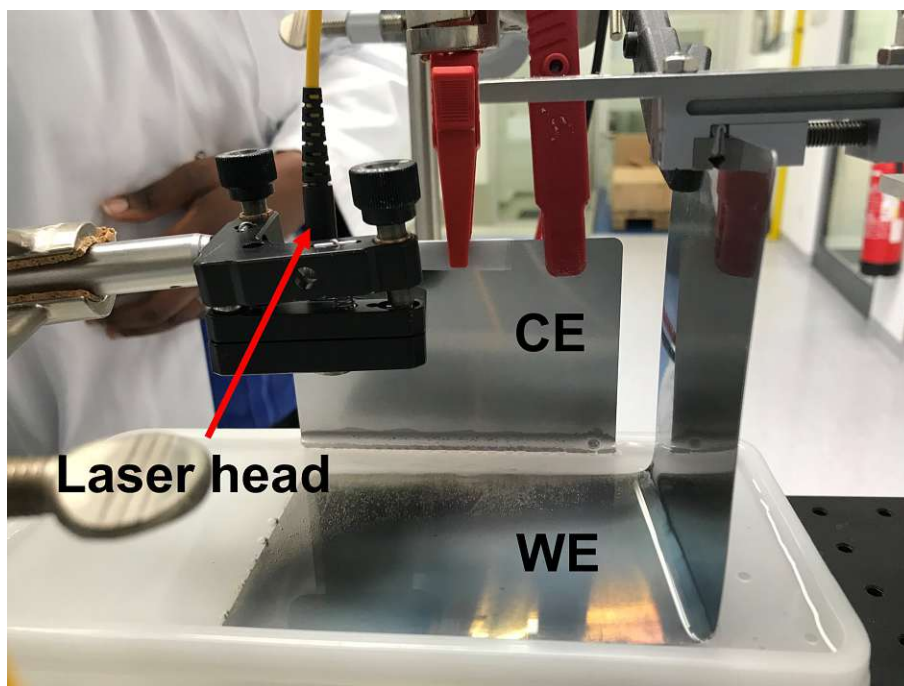
Figure 7.2: Experimental setup for the in situ zinc layer thickness measurement with laser interferometry. The arrangement of the laser head, the working electrode (WE) and the counter electrode (CE) can be seen.

and the sensor head. The data was recorded and evaluated later. The Layer thickness is calculated from the difference to the original distance (distance before the deposition started).

7.3 Results and discussion

In our basic idea, the standardised Hull cell was to be converted. We wanted to make it possible to measure the layer thickness by means of a laser interferometer during deposition in the hull cell. For this purpose, the Hull cell standardised in Germany with the DIN standard DIN 50957 was rebuilt using CAD software and then 3D printed with polypropylene (see Figure 7.3). We have installed a window in the longest side of the Hull cell. To do this, we first integrated a viewport at the end of which a 1λ fused silica uncoated glass (12.5 mm diameter, 2 mm thickness) was glued to create the window so that no solution leaks from the cell. The working conditions are very harsh, as we work in strongly alkaline media. For the selection of the materials we had to make sure that they have a certain resistance to pH values above 12. Therefore, the material for the production of the cell, the glass for the

window as well as the glue to fix the glass to the viewport are resistant to strong alkaline media.

The viewport is aligned perpendicular to the cathode. The viewport should also not penetrate too deeply into the cell, so as not to hinder the flow too much in the low current density range. Figure 7.3 shows the trend of the field lines between the anode and the cathode when the Hull cell is modified with a window. It shows that the field lines in the low current density side could be distorted if the viewport penetrates too deep into the cell. The material of the tube can act as a physical barrier for the ion flow.

Depositions of zinc were successfully carried out with the new cell, using the standard conditions described in the Experimental section 7.2. However, when the in situ measurements of thickness were attempted there were a number of challenges. We first found that the viewport was too narrow and therefore the laser beam could not be aligned properly. Once this challenge had been overcome by adjusting the viewport diameter, the sensor head could be aligned in air to reflect off the steel test sheet and obtain a signal strong enough for testing. Adding the electrolyte to the bath, however, caused the signal intensity to decrease dramatically. Although it was hypothesised that the refractive index change could perhaps have changed the alignment, no amount of realignment could re-establish a suitable signal intensity. It was found that with the full amount of liquid, no layer thickness could be measured due to the strong absorption of water. The absorption in water in the infrared spectral range is particularly high. Therefore, in our case, using an IR laser made the measurement impossible. Furthermore, it was also very difficult to ensure a reasonable alignment of the laser beam, despite the flexibility of the optical fibre supplying the laser head. Therefore, another way to improve the set up would be to add flexibility or a much wider opening into the window tube so that the laser could be adjusted more easily. There was also a strong reflection on the glass window, which could perhaps be reduced with suitable anti-reflection coatings. All these aspects led to the failure of the experiment. Therefore, we had to rethink the experiment.

In order to make the proof of principle experiment we decided the best strategy was to eliminate the windows and drastically reduce the amount of liquid. Therefore, we designed an experiment geometry which captured a similar electrode positioning to that of the Hull cell

but without the restrictions of the electrolyte volume and vertical positioning of the electrodes within the Hull cell. Our solution was to use a low walled, shallow container (specifically the lid of a plastic box) as shown in Figure 7.2. The working electrode could then be laid horizontally into the bottom of the plastic lid. Not using the designed cell eliminated the restriction of the viewport. This allowed us to align the laser above the sample sheet and record a changing thickness from the laser interferometer. Finally, the experiment was successful.

Figure 7.4 shows the data recorded during the experiment. Apart from the device noise, one can clearly see that the layer thickness increases with time. The device disturbances are caused by vibrations in the environment and the device itself. During zinc deposition, hydrogen gas is evolved, which also lead to additional disturbances of the measurement. The laser is very sensitive and the hydrogen evolution leads to a change in the refractive index of the solution to be measured, because hydrogen has a different refractive index compared to the sample solution. Steps can also be seen in the plot in Figure 7.4. These are also attributed to hydrogen evolution. With large hydrogen bubbles, the steps are also larger because the distance between the laser head and the sample decreases considerably, because the laser is measuring the bubble at this moment. When the bubble disappears, the laser measures the deposited layer again. If the hydrogen bubbles are small, the steps are correspondingly small. The deposition at the beginning seems to be faster than later during the deposition reaction. The slope of the linear fit for the reaction begin is 46% (red line), while it's 6% for the rest of the reaction (Blue line). This is in accordance with what we were discussing in the Chapters 4 and 5. We first have a first deposition with the depletion of the polymer and then further deposition is limited by barrier effect of the adsorbed polymer.

A comparison between these values and the values of a sheet coated in the standardised Hull cell is impossible. Mainly because the experimental setup or the arrangement of the electrodes is not the same. Furthermore, the course of the field lines is also different due to the new arrangement of the anode to the cathode. The values recorded in Figure 7.4 are in the range up to 120μm,while the layer thickness of the standard Hull cell sheets are in the range between 4 and 6.5μm. The value 120μm is the one set as 100% for plot in 7.4. It makes sense that the layer thickness of the normal sheets is smaller than that

recorded in Figure 7.4. In the normal Hull cell, the distance between
the cathode and anode is greater than that in the experiment with the
laser interferometer. There is also an additional parameter that will
explain the difference in the measured thicknesses. The interferometry
device measures the distance between the sensor head and the reflec-
tive layer without taking in account the environment. It only uses air
as the environment. In this case we have air, then water (electrolyte)
and finally the reflective layer. The detector software doesn't give the
possibility to set any environment material or materials in a layered
system like we have. So the thickness measured here is an estimated
value. For future works it should be possible to consider programming
this features with a tool like SFA explorer.

It is important to note that with the normal Hull cell sheet, the
thickness distribution was measured over the entire sheet. Whereas
in the laser interferometry experiment, the layer thickness was only
measured at one point. We only had one laser head to carry out the
experiment and could therefore only measure one spot on the sheet at a
time. To measure the layer distribution on the sheet with this method,
we would either have to have several laser heads that we fix on the
sample at the same time, or the other possibility is to have one laser
head, which we fix on a movable frame in order to move the laser head
on the same X-axis over the whole steel sheet.

7.4 Conclusion

It is very important to be able to control the deposition of a layer. But
it is also very important to be able to determine the thickness of the
deposited layer. The layer thickness influences various properties of a
coating, such as the optical appearance, the mechanical and electrical
properties and the corrosion protection properties. There are already
enough methods to measure layer thickness after the deposition is
finished (ex-situ methods). However, an innovative idea would be to
be able to measure the layer while it is still being deposited. This will
be interesting for the electroplating industry in that it will help them
to be faster in controlling the quality of the electrolyte. In the course
of this work, we have demonstrated it is possible to measure the zinc
layer in real time. Although there were difficulties in carrying out the
experiment directly in the Hull cell, we managed to offer a solution

using a modified, more open geometry.

However, we still propose that in situ measurements in the Hull cell could still be carried out successfully with some modified conditions. For example, the intensity could be increased by either changing the wavelength of the laser or the power. Even if this approach could lead to further problems, it is likely that they can be mitigated. Potential problems would be, for example, the layer thickness that can be probed, which is wavelength dependent, could become out of range if the wavelength is changed. Also, increasing the power could lead to heating of the system, which could be mitigated with cooling.

Another solution for the feasibility of the experiment in a Hull cell would be to bend the sample sheet inward from above at an angle of about 10 degrees and cover the sheet completely with the electrolyte. Of course the bent part should be covered only with a very thin layer of the liquid. Then you could hang the laser head over it and bring it very close to the sheet without touching the solution.

If further research is made into this subject, then we could reach the point where the method is adapted to the industrial electroplating unit. This is actually the goal that should be achieved. The first step would be to be able to perform the experiment in the Hull cell. The second step would be to couple the Hull cell experiment to the industrial electroplating system. For example, one could put a small outlet/inlet in the electroplating tank that would carry the electrolyte from the large electroplating tank over to the Hull cell. In the Hull cell there would also be a small inlet/outlet that would allow the solution to pass from the cell to the large tank. This setup should result in a constant flow through the cell. While the metal deposition takes place in the large tank, parallel Hull cell experiments could be made. This would directly find out if there is a problem with the galvanic bath. Since the Hull cell allows the tracking of the consumption of the bath components and the adjustment of the bath accordingly.
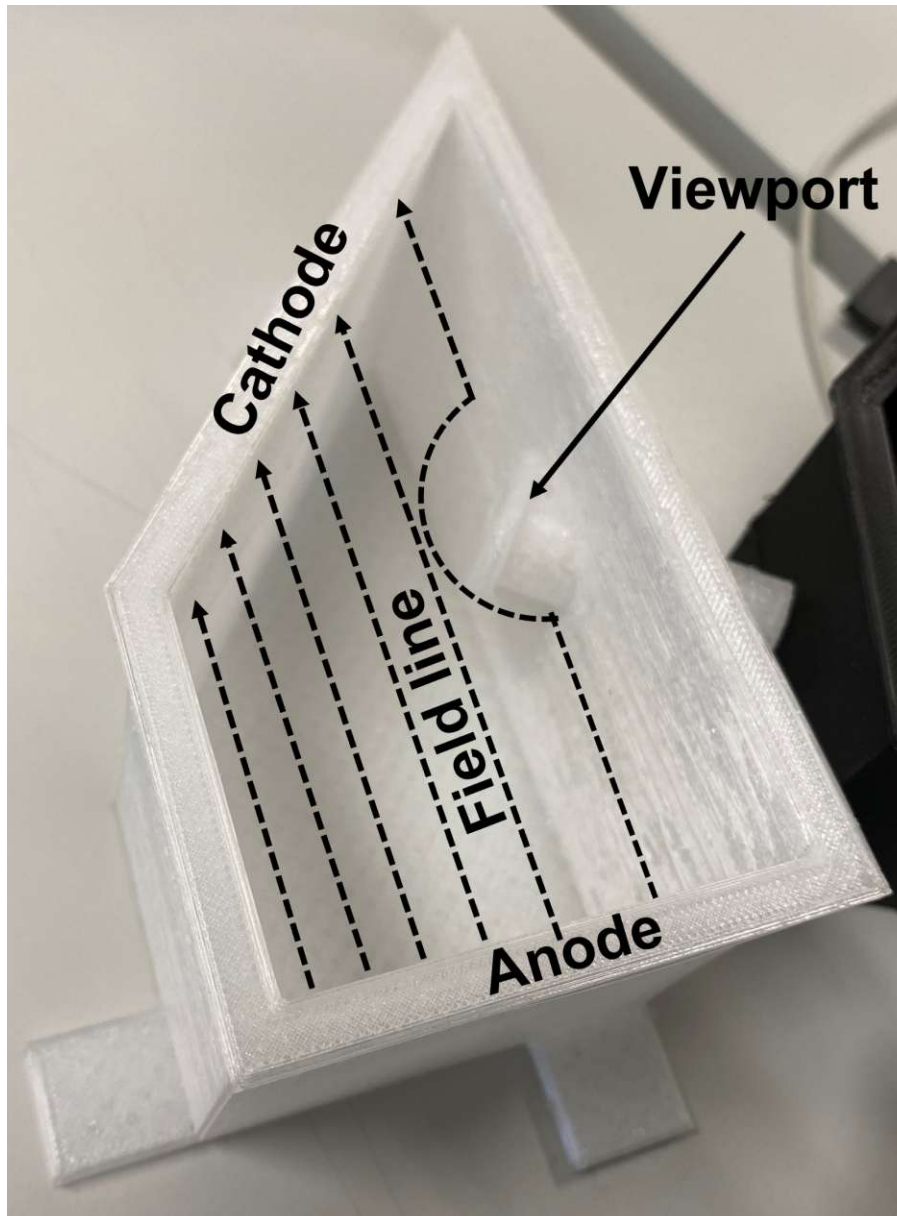
Figure 7.3: Trend of the field lines in the adapted 3D printed Hull cell. The viewport could disturb the ion flow and cause a deformation of the field lines.
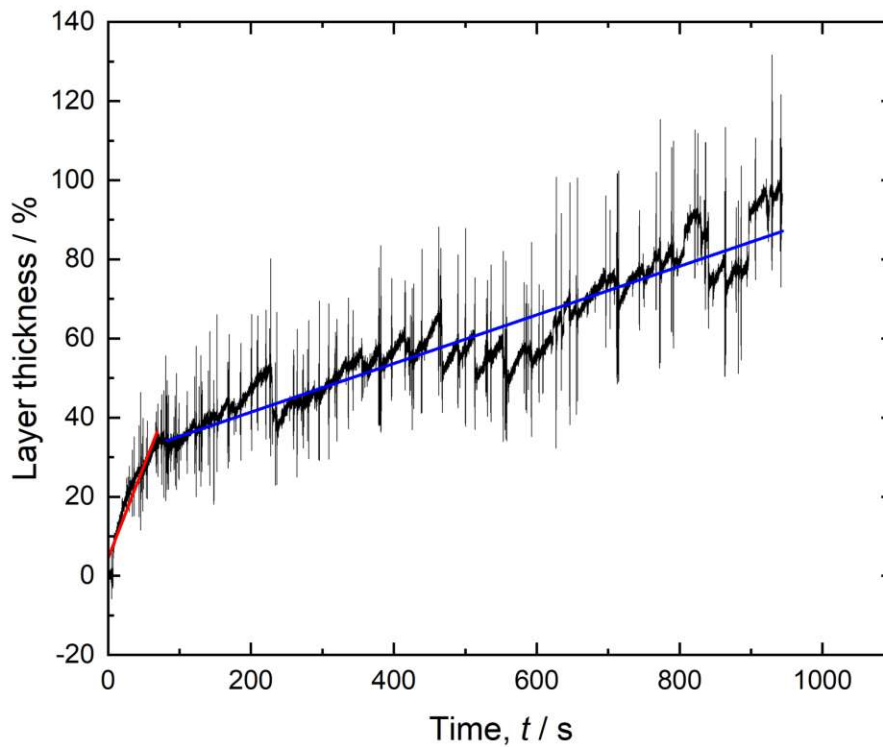
Figure 7.4: Layer thickness measured in real time during zinc deposition. The thicknesses are estimated values and are therefore evaluated in percent, while using the last stable value as 100%. The linear fit in blue has a slope of 6% and the red has a slope of 46%

8 Conclusion and Outlook

In this work we have used methods such as cyclic voltammetry, QCM-D, XPS, AFM and LEIS to understand the role, the influence and the moderation mechanism of polyquaternium 2 in an alkaline cyanide free zinc bath. The plan was to use this knowledge to be able to produce a polymer that performs better than conventional, commercially available, poly quaternary ammonium polymer additives. The main results of this research are summarised in Figure 8.1.

Poly quaternary ammonium polymers have been successfully used in electroplating for some time. Until now, the investigations on the subject had only shown which polymers positively influence the deposition and that these polymer additives transport the zincate ions to the metal surface and inhibit the metal deposition. However, there was nothing, for example, about the crystal structure of the deposited zinc layer. Therefore, the first objectives of this dissertation were to fundamentally understand the effect of poly quaternary ammonium polymers on the electrochemical deposition of zinc and to find out the mechanism by which the polymer controls the deposition. Chapter 4 shows how we achieved these goals by performing cyclic voltammetry and QCM-D and XPS experiments. The role of the polymer in the alkaline zinc bath, the kinetics of deposition and the mechanism of adsorption were elucidated.

It was found that the polymer transports the zincate anions to the metal surface where they are reduced. The fact that the zincate interacts with the polymer to form a zincate loaded polymer matrix is confirmed by XPS spectra. Then we can clearly observe, in the spectra, a peak from the ZP electrolyte analysis that we assigned to the zincate adsorbed within the polymer. Owing to electrostatic repulsion this adsorption within the polymer is necessary to facilitate the approach of the negatively charged zincate to the negatively charged surface of the electrode. This way the zincate can access the inner sphere of the electric double layer. In the process, the zincates in the polymer are
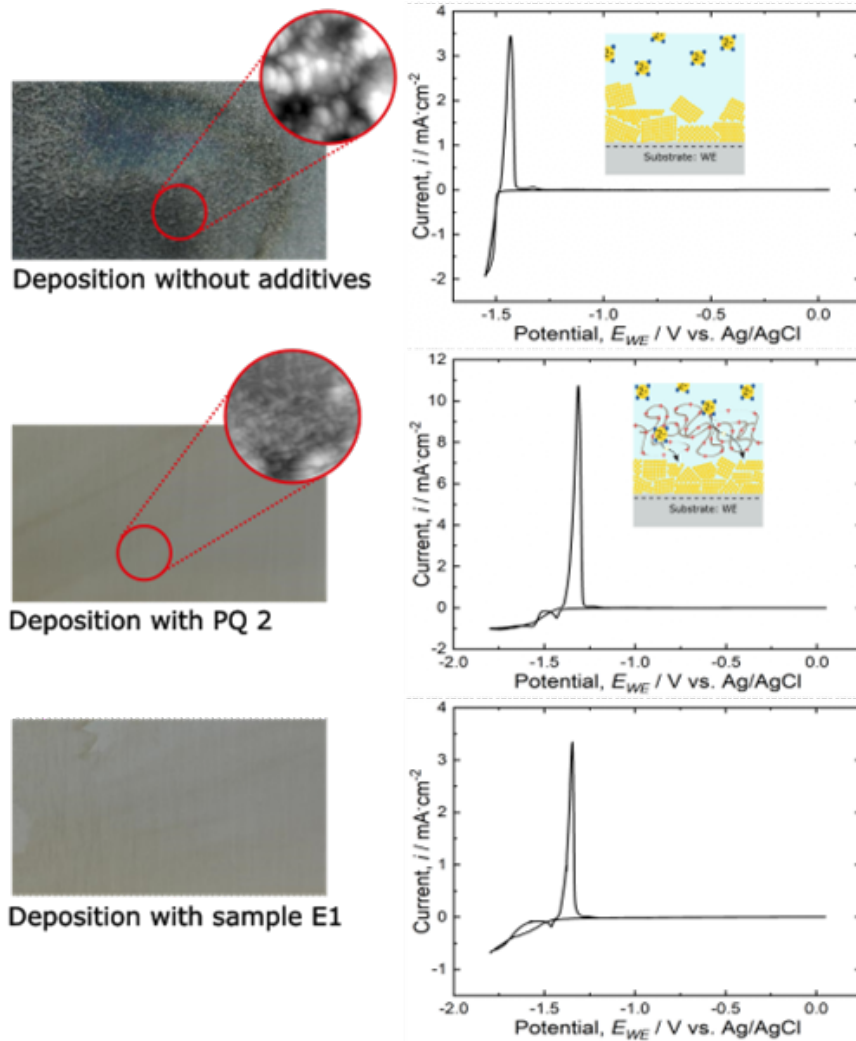
Figure 8.1: Sketch showing the difference induce through adding a poly quaternary ammonium polymer to the alkaline cyanide free electrolyte.

consumed (reduction reaction) first, when they enter the inner sphere of the electric double layer. Afterwards the polymer is adsorbed at the electrode interface and forms a physical barrier for the remaining zincate ions, so that further reduction reactions happen through diffusion of the zincate through the polymer layer.

Another aim of this work was to find out why polyquaternium 2 improves the quality of the deposited layer. This question is answered with the help of AFM and LEIS investigations (see chapter 5). We were able to image the surface of the zinc layer deposited with and without polyquaternium 2 and see the morphology of the layer. The electrostatic charges of the surface condition the crystal growth mechanism.

When there is no polymer additive in the zinc bath the deposited layer is rough, uneven and shows different grain sizes. The imaging shows that nucleation started at difference position at the surface and islands are created, when the growth mechanism continues on top of those initial nucleation sites. This type of growing mechanism is called the Volmer-Weber-growth mechanism. The presence of the polymer at the interface overscreens the surface charge and transforms the island crystal growth to more of a layer-by-layer (Stranski-Krastanov) crystal growth mechanism, where the layer-by-layer growth dominates the island growth at the beginning of the deposition before turning to the island growth for later layers. The LEIS measurement confirms that there is an alloying of the zinc with the gold already from the beginning of the deposition reaction. Imaging the surface of the layer shows that the layer is smooth, even and consisted of elongated grains of an approximately the same size. Thanks to AFM investigations we were able to see how polyquaternium 2 adsorbs at a negatively charged surface specially mica. This brought additional explanation on how the polymer additive controls the crystal growth. The ex-situ AFM of the polymer at the surface of mica shows that the polymer forms island of polymer, which consist on several chains per island. In wet condition the island are more expand at the surface than in dry conditions. In the elctrolyte the polymer will provide a good coverage of the surface and this way enable the initial deposition to distribute zinc atoms everywhere.

We were also able to synthesise a poly quaternary ammonium polymer (see Chapter 6) that works at least as well as polyquaternium 2. This is verified with the cyclic voltammetry, that shows that both polymer (self made and polyquartenium 2) strongly moderate the zinc deposition. We saw that sample E1 inhibits stronger in the high current density than polyquaternium 2. The success of the synthesis was confirmed by the molecular weight distribution, that shows that the average molecular weight of the self made polymer is about 15000 Da while polyquaternium 2 is about 20000 Da. The chemical structure of both (polyquaternium 2 and self made polymer) polymers differs only in the crosslinker used for the polymerisation. The IR bands confirm this statement. The crosslinker in the self made polymer has respectively one more ethyl-group and ether-group in his backbone and therefore it is more flexible in its structure. This leads to more flex-

ibility in the backbone chain of the synthesised polymer. Comparing the layer thickness deposited in the presence of each polymer shows that the self made polymer inhibits more at high current density than polyquaternium 2. Both layers are shiny and smooth. However, the layer deposited from the self made polymer is yellowish, due to the polymer colour.

By carrying out experiments in a Hull Cell, a method was developed in Chapter 7 to measure the layer thickness of zinc in real time during deposition. For our project we used the standard Hull cell and redesigned the body to adapt it to our idea. Various parameters have led to the proof of principal not being successful in the so-called Hull cell. Nevertheless, we were able to carry out the measurement in a provisional format. This method and how it works allows the writing of a patent, that is in preparation.

This thesis is coming to an end and I hope that I have stimulated the curiosity of at least one person to further investigate the subject of the moderation of zinc electroplating by polyquaternary ammonium polymers. Even if we've been able to answer some crucial questions on the subject, some reflections deserve to be explored in greater depth. For the future, investigations on compounds that only influence the reaction in high or in low current density can be interesting. What kind of polymer can accelerate or inhibit the deposition reaction in a way that, we achieve the ideal case where the layer thickness distribution across the Hull cell sheet stays constant? Commercially available polymer additives that are used as levellers are mainly effective in the high current density sites. We are convinced that the key to resolve this problem involves the variation of the molecular weight of the polymer. This will help to control the diffusion at the different field gradients. Creating for example polyquaternary ammonium polymer with shorter chains can probably be a good option to influence the zinc deposition in the low current density sites.

During this work we were only able to look at ex-situ AFM images of the zinc deposition and the polymer on mica and therefore couldn't answer all the opened questions that motivate this work. Investigating the in-situ deposition reaction can be the solution to finally be able to know: what compounds can accelerate the deposition reaction in low current density and at the same time inhibits the reaction in the high current density? Using a method like surface force apparatus

(SFA) can help in answering this question. Because it is a method that can help characterising the polymer layer in real time during the deposition reaction. We have performed a multitude of experiments with the SFA method. During this investigation we were able to adapt the measuring cell to our high pH electrolyte by replacing the base of the cell with polycarbonate, Which is a material that is resistant to high pH environment. However, due to time constraints we were unable to obtain any conclusive results. Therefore, we are confident that this method could be very useful for future work on this topic.

9 Appendix

9.1 Appendix A: IR spectra of the polymer additives

The Figure 9.1 shows the IR spectra of the two examined polymers self made polymer sample E1 and PQ2 with the respective functional groups assigned to the bands. The following signals can be seen in the respective spectra:

- 3320 cm⁻1: N-H stretching vibration of the amine group and amide group.

- 3000-2800 cm⁻1: C-H stretching vibrations of aliphatic groups

- 1653 cm⁻1: C=O stretching vibration of the amide group

- 1556 cm⁻1: N-H bending vibration of the amine group

- 1471 cm⁻1: C-H bending vibration of the methyl groups

- 1256 cm⁻1: C-N stretching vibration of the amine group

- 1120 cm⁻1 and 1066 cm⁻1: C-O stretching vibration of the ether group

- 980-750 cm⁻1: C-H bending vibration of aliphatic groups

- 515 cm⁻1: N-Cl stretching vibrations

Due to the presence of additional aliphatic groups or the second ether group due to the modified cross-linker, the respective bands (3000-2800 cm⁻1, 1120 cm⁻1, 1066 cm⁻1, 980-750 cm⁻1) are more significantly visible in sample E1. In addition to the above bands, the bands of a C=O stretching vibration (1751 cm⁻1) and an O-H bending vibration (1353 cm⁻1) are visible in the sample E1. These bands probably show a slight contamination of the sample with a carboxylic acid.

The IR data obtained are consistent with the structures of the polymers studied, with great similarities between the two polymers. Due to the change of the cross-linker to two ether groups (in sample E1), the aliphatic bands or ether bands are more intensively visible and therefore show the successful exchange of the cross-linker. In contrast, in the polymer PQ2 the signal part in the range 3320 cm-1 is a little more pronounced, which can be well explained by the higher (relative) proportion of amine and amide groups in the polymer. In addition

to the clearly assignable signals, two weak bands (1751 cm^{-}1, 1353 cm^{-}1) are found, which indicate carboxylic acids and possibly point to a slight impurity or a production residue. All relevant elements of the two polymers, as well as their different intensities, were detected in the course of the investigation. According to the IR data, it can be assumed that the two structures are correct and that the two samples are of high purity.
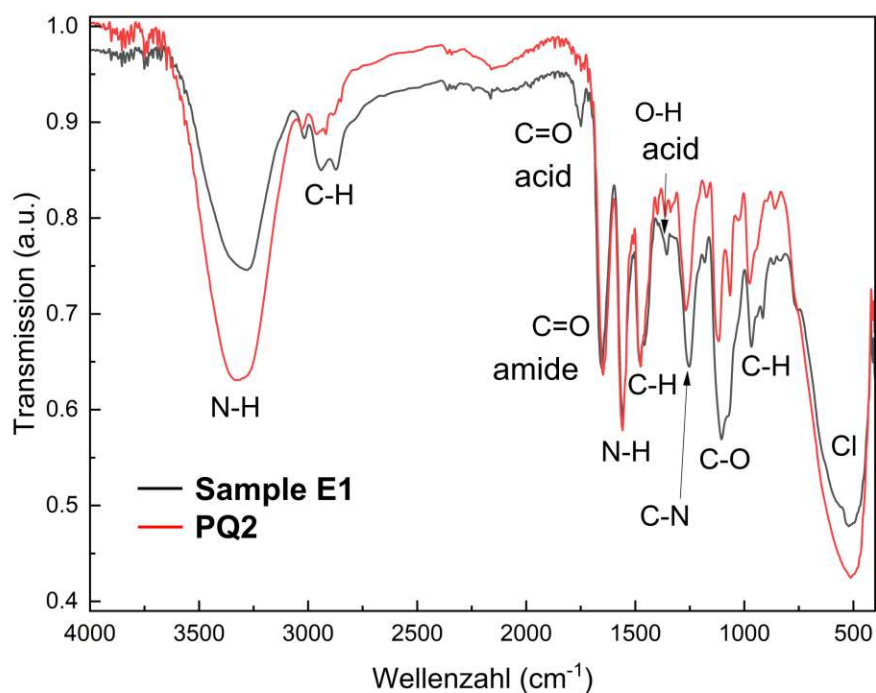

Figure 9.1: Infrared spectra of the synthesised polymer sample E1 in black and polyquarternium 2 in red

9.2 Appendix C: Curriculum Vitae

Raabestrasse 3
58313 Herdecke

Mobil: 0176/70166714
gasteltietcha@hotmail.com

Gastelle Tiétcha

Persönliche Informationen

Familienstand	ledig
Nationalität	deutsch
Geburtsdatum	10.03.1991
Geburtsort	Douala, Kamerun

Schulbildung

1996 - 2000	Grundschule in New-Bell, Douala
2000 - 2007	Lycée de New-Bell, Douala **Abschluss: Abitur in den Fächern Biologie, Chemie und Mathematik**
2007 - 2008	Deutschkurs am Goethe Institut in Yaoundé, Kamerun **Abschluss: Zertifikat Deutsch**

Studium

April - Juli 2009	Deutschkurs an der Goethe Universität in Frankfurt am Main **Abschluss: Deutsche Sprachprüfung für den Hochschulzugang**
Okt. 2009 - März 2012	Studium der Chemie an der Goethe Universität in Frankfurt
April 2012 - Sept. 2014	Studium der Chemie an der Justus-Liebig-Universität in Giessen **Abschluss: Bachelor of Science**
Okt. 2014 - Juni 2017	Studium der angewandten Polymerwissenschaften an der FH Aachen **Abschluss: Master of Science**
April 2018 – Dec. 2023	Doktoratsstudium der technischen Wissenschaften Technische Physik an der TU Wien: Bei Prof. Dr. Markus Valtiner

Arbeitserfahrung

Aug. 2009 – Nov. 2010	Aushilfe im Gastronomie Service
Feb. 2011 – Okt. 2014	Aushilfe im Gastronomie Service
März 2011	Praktikum bei der Flora Apotheke in Maintal
Mai 2012 - Mai 2013	Call-Center-Agentin bei Tradelog Instore-Services GmbH (Bewerberkontakt für Dienstleistungen)
Juni 2015 - Mai 2016	Wissenschaftliche Mitarbeiterin am Institut für Textiltechnik in Aachen
März 2016 - Juli 2016	Wissenschaftliche Mitarbeiterin bei M-Base Engineering & Software GmbH (überwiegend Pflege einer Datenbank)
Aug. 2016 - Mai 2017	Masterarbeit bei Dörken Coatings GmbH & Co. KG
Mai 2017 - Dez. 2021	Doktorandin bei Dörken Coatings GmbH & Co. KG
Seit Mai 2023	Mitarbeiterin in der Forschung und Entwicklung bei CHEMOPUR GmbH

87

9 Appendix

Sprachkenntnisse

Französisch   Muttersprache

Deutsch   fließend in Wort und Schrift

Englisch   sehr gute Kenntnisse

EDV-Kenntnisse

MS-Office (Word, Excel, PowerPoint), Origin, CATIA

Veröffentlichungen

Hong, L.; Ahles, S.; Heindl, A. H.; Tiétcha, G.; Petrov, A.; Lu, Z.; Logemann, C.; Wegner, H. A. An air-stable bisboron complex: a practical bidentate Lewis acid catalyst. Beilstein J. Org. Chem. 2018, 14, 618–625.

Tiétcha, G.F.; Mears, L.L.E.; Dworschak, D.; Roth, M.; Klüppel, I.; Valtiner, M. Adsorption and Diffusion Moderated by Polycationic Polymers during Electrodeposition of Zinc. ACS Appl Mater Interfaces. 2020, 12(26), 29928-29936.

Tiétcha, G.F.; Klüppel, I.; Kogler, M.; Valtiner, M.; Mears, L.L.E. Visualizing electrochemical zinc deposition and the role of a polymer additive in the crystal growth mechanism. Mater. Corros. 2023, 1–10.

Private Interessen

Seifenherstellung, Herstellung von Naturkosmetik, Freunde treffen, Musik hören

9.3 Appendix D: Copyright clearances

No additional permission was required as the paper is licensed under a Creative Commons Attribution license CC-BY.

References

[1] R.C. Snowdon. Electrolytic precipitation of zinc. *J. Phys. Chem.*, 11:369–381, 1907.

[2] M. Li, S. Luo, Y. Qian, W. Zhang, L. Jiang, and J. Shen. Effect of additives on electrodeposition of nanocrystalline zinc from acidic sulfate solutions. *Journal of The Electrochemical Society*, 154: D567–D571, 11 2007.

[3] J.-Y. Lee, J.-W. Kim, M.-K. Lee, H.-J. Shin, H.-T. Kim, and S.-M. Park. Effects of organic additives on initial stages of zinc electroplating on iron. *J. Electrochem. Soc.*, 151, 01 2004.

[4] M. Pushpavanam. Role of additives in bright zinc deposition from cyanide free alkaline baths. *J. Appl. Electrochem.*, 36(3):315–322, 2006. ISSN 0021-891X.

[5] A. Rethinam, G. Ramesh Bapu, and V. Muralidharan. Role of addition agents in zincate bath- a cyclic voltammetry study. *Trans. Inst. Met. Finish.*, 81(4):136 – 140, 2003.

[6] J. L. Ortiz-Aparicio, Y. Meas, G. Trejo, R. Ortega, T. W. Chapman, E. Chainet, and P. Ozil. Effect of aromatic aldehydes on the electrodeposition of znco alloy from cyanide-free alkaline-gluconate electrolytes. *J. Appl. Electrochem.*, 41(6):669–679, 2011. ISSN 0021-891X.

[7] J. L. Ortiz-Aparicio, Y. Meas, T. W. Chapman, G. Trejo, R. Ortega, and E. Chainet. Electrodeposition of zinc in the presence of quaternary ammonium compounds from alkaline chloride bath. *Journal of Applied Electrochemistry*, 45:67 – 78, 2015.

[8] T.W. Jelinek. *Hull-Zelle zur Untersuchung von galvanischen Elektrolyten*. Eugen G. LEUZE Verlag, 1 edition, 2007. ISBN 978-3-87480-224-6.

References

[9] P. W. Atkins, J. de Paula, and J. J. Keeler. *Physikalische Chemie*. Wiley-VCH, 6 edition, 2021. ISBN 978-3-527-34550-2.

[10] G. Kaltenpoth. *Elektrochemische Prozesse an strukturierten Substraten für Anwendungen in neuartigen Leitungstechnologien*. PhD thesis, Ruprecht - Karls - Universität Heidelberg, 2003.

[11] X. Jin and K. Huang. Precautions of using three-electrode configuration to measure electrode overpotential in solid oxide electrochemical cells: Insights from finite element modeling. *Journal of The Electrochemical Society*, 167(12):124501, aug 2020.

[12] W. Schmickler. Electrochemical theory: Double layer. In *Reference Module in Chemistry, Molecular Sciences and Chemical Engineering*. Elsevier, 2014. ISBN 978-0-12-409547-2.

[13] A. T. Celebi, M. Olgiati, F. Altmann, M. Kogler, L. Kalchgruber, J. Appenroth, U. Ramach, M. Valtiner, and L. L. E. Mears. Experimental and theoretical understanding of processes at solid-liquid interfaces at molecular resolution. In *Reference Module in Chemistry, Molecular Sciences and Chemical Engineering*. Elsevier, 2023.

[14] N.B. Khojasteh, S. Apelt, U. Bergmann, S. Facsko, and R. Heller. Revealing the formation dynamics of the electric double layer by means of in-situ rutherford backscattering spectrometry. *Rev Sci Instrum.*, 90:085107–085107, 2019.

[15] W. J.L. Plieth. *Der galvanische Prozess: Grundlagen der Metallabscheidung und Strukturbildung*. Eugen G. Leuze Verlag KG, 1 edition, 2018. ISBN 978-3-87480-346-5.

[16] W. J. Lorenz and G. Staikov. 2d and 3d thin film formation and growth mechanisms in metal electrocrystallization - an atomistic view by in situ stm. *Surface Science*, 335:32 – 43, 03 1995.

[17] N. Kaiser. Review of the fundamentals of thin-film growth. *Applied Optics*, 41(16):3053 – 3060, 06 2002.

[18] S. Artemev. Investigation of mechanisms of the crystal growth process (kossel model). *Technology audit and production reserves*, 3:4–10, 01 2018.

[19] K. A. Jackson. *Theory of Crystal Growth*, pages 233–282. Springer US, Boston, MA, 1975.

[20] J. Yoreo and P. Vekilov. Principles of crystal nucleation and growth. *Reviews in Mineralogy & Geochemistry - REV MINERAL GEOCHEM*, 54:57–93, 01 2003.

[21] P. Cubillas and M. Anderson. *Synthesis Mechanism: Crystal Growth and Nucleation*, volume 1, pages 1–55. WILEY-VCH Verlag GmbH & Co. KGaA, 06 2010. ISBN 9783527325146.

[22] S. Papaleo, M. Rovitto, and H. Ceric. Mechanical effects of the volmer-weber growth in the tsv sidewall, 2016. IEEE 66th Electronic Components and Technology Conference.

[23] C. Fornari, G. Fornari, P. Rappl, E. Abramof, and J. Travelho. *Monte Carlo Simulation of Epitaxial Growth*, chapter 5. IntechOpen, 03 2018. ISBN 978-953-51-3889-1.

[24] H. Heo, J. H. Sung, J.-H. Ahn, F. Ghahari, T. Taniguchi, K. Watanabe, P. Kim, and M.-H. Jo. Frank–van der Merwe Growth versus Volmer–Weber Growth in Successive Stacking of a Few-Layer Bi_2Te_3/Sb_2Te_3 by van der Waals Heteroepitaxy: The Critical Roles of Finite Lattice-Mismatch with Seed Substrates. *Adv. Electron. Mater.*, 3(1600375):7, 2017.

[25] S. Ossicini, R. Memeo, and F. Ciccacci. Aes analysis of the growth mechanism of metal layers on metal surfaces. *Journal of Vacuum Science & Technology A: Vacuum, Surfaces, and Films*, 3:387 – 391, 04 1985.

[26] A. Yli-Pentti. *4.11 - Electroplating and Electroless Plating*, pages 277–306. Elsevier, Oxford, 2014. ISBN 978-0-08-096533-8.

[27] M. Mittal, S. Sardar, and A. Jana. Chapter 7 - nanofabrication techniques for semiconductor chemical sensors. In C. M. Hussain and S. K. Kailasa, editors, *Handbook of Nanomaterials for Sensing Applications*, Micro and Nano Technologies, pages 119–137. Elsevier, 2021. ISBN 978-0-12-820783-3.

[28] J. M. G. Cowie and V. Arrighi. *Polymers: Chemistry and Physics of Modern Materials*. CRC Press, 3 edition, 2007. ISBN 9780429125546.

[29] I. Teraoka. *Polymer Solutions: An Introduction to Physical Properties*. John Wiley & Sons, Inc., 1 edition, 2002.

[30] M. Pönitsch. *Rheo-optische Experimente zur Hydro und Thermodynamik von Polymeren in verdünnten Lösungen*. PhD thesis, Technischen Universität Berlin, 1999.

[31] R. Wang and Z.-G. Wang. Theory of polymers in poor solvent: Phase equilibrium and nucleation behavior. *Macromolecules*, 45 (15):6266–6271, 2012.

[32] F. Li and F. Pincet. Confinement free energy of surfaces bearing end-grafted polymers in the mushroom regime and local measurement of the polymer density. *Langmuir*, 23(25):12541–12548, 2007. ISSN 0743-7463.

[33] E. L. P. Dumont, H. Belmas, and H. Hess. Observing the mushroom-to-brush transition for kinesin proteins. *Langmuir*, 29(49):15142–15145, 2013.

[34] I. M. Ismail, O. E. Abdel-Salam, T. S. Ahmed, A. Soliman, M. F. Al-Ebrahim, and I. A. Khattab. Investigation of the anodic dissolution of zinc in sodium chloride electrolyte- a green process. *IOSR Journal of Applied Chemistry*, 6(3):24 – 32, 2013.

[35] M. Mokaddem, P. Volovitch, and K. Ogle. The anodic dissolution of zinc and zinc alloys in alkaline solution. i. oxide formation on electrogalvanized steel. *Electrochim. Acta*, 55(27):7867–7875, 2010. ISSN 0013-4686.

[36] T. N. Vu, M. Mokaddem, P. Volovitch, and K. Ogle. The anodic dissolution of zinc and zinc alloys in alkaline solution. ii. al and zn partial dissolution from 5 *Electrochim. Acta*, 74:130–138, 2012. ISSN 0013-4686.

[37] T. J. Tuaweri, E. M. Adigio, and P. P. Jombo. A study of process parameters for zinc electrodeposition from a sulphate bath. *IJESI*, 2(8):17–24, 2013.

[38] T. V. Byk, T. V. Gaevskaya, and L. S. Tsybulskaya. Effect of electrodeposition conditions on the composition, microstructure, and corrosion resistance of zn–ni alloy coatings. *Surf. Coat. Technol.*, 202(24):5817–5823, 2008. ISSN 0257-8972.

[39] M. Gavrila, J. P. Millet, H. Mazille, D. Marchandise, and J.M. Cuntz. Corrosion behaviour of zinc–nickel coatings, electrodeposited on steel. *Surf. Coat. Technol.*, 123(2):164–172, 2000. ISSN 0257-8972.

[40] H. Kim, B. N. Popov, and K. S. Chen. Comparison of corrosion-resistance and hydrogen permeation properties of zn–ni, zn–ni–cd and cd coatings on low-carbon steel. *Corros. Sci.*, 45(7):1505–1521, 2003. ISSN 0010-938X.

[41] C. Shen, X. Li, N. Li, K. Xie, J.-G. Wang, X. Liu, and B. Wei. Graphene-boosted, high-performance aqueous zn-ion battery. *ACS Appl. Mater. Interfaces*, 10(30):25446–25453, 2018. ISSN 1944-8244.

[42] T. Foroozan, V. Yurkiv, S. Sharifi-Asl, R. Rojaee, F. Mashayek, and R. Shahbazian-Yassar. Non-dendritic zn electrodeposition enabled by zincophilic graphene substrates. *ACS Appl. Mater. Interfaces*, 11(47):44077–44089, 2019.

[43] P. Moreno-García, N. Schlegel, A. Zanetti, A. Cedeño López, M. de Jesús Gálvez-Vázquez, A. Dutta, M. Rahaman, and P. Broekmann. Selective electrochemical reduction of co2 to co on zn-based foams produced by cu2+ and template-assisted electrodeposition. *ACS Appl. Mater. Interfaces*, 10(37):31355–31365, 2018. ISSN 1944-8244.

[44] G. Tian, M. Zhang, Y. Zhao, J. Li, H. Wang, X. Zhang, and H. Yan. High corrosion protection performance of a novel nonfluorinated biomimetic superhydrophobic zn–fe coating with echinopsis multiplex-like structure. *ACS Appl. Mater. Interfaces*, 11(41): 38205–38217, 2019. ISSN 1944-8244.

[45] S.-D. Han, N. N. Rajput, X. Qu, B. Pan, M. He, M. S. Ferrandon, v Liao, K. A. Persson, and A. K. Burrell. Origin of electrochemical, structural, and transport properties in nonaqueous zinc electrolytes. *ACS Appl. Mater. Interfaces*, 8(5):3021–3031, 2016. ISSN 1944-8244.

[46] T.W. Jelinek. *Galvanische Verzinkung. Elektrolyte, Nachbehandlung, Anwendung*. Eugen G. LEUZE Verlag, 1 edition, 2003. ISBN 3-87480-179-9.

References

[47] J. S. Fordyce and R. L. Baum. Vibrational spectra of solutions of zinc oxide in potassium hydroxide. *J. Chem. Phys.*, 43(3):843–846, 1965. ISSN 0021-9606.

[48] G. H. Newman and G. E. Blomgren. Nmr study of complex ions in the aqueous zno–koh system. *J. Chem. Phys.*, 43(8):2744–2747, 1965. ISSN 0021-9606.

[49] T. P. Dirkse. The nature of the zinc-containing ion in strongly alkaline solutions. *J. Electrochem. Soc.*, 101(6):328 – 331, 1954.

[50] A. N. Maslii, M. S. Shapnik, and M. Kuznetsov. Electroreduction of zn(ii) hydroxy-complexes in aqueous electrolytes: A quantum-chemical study. *Russ. J. Electrochem.*, 37(6):615 – 622, 2001.

[51] Heinz Gerischer. Mechanism of electrolytic deposition and dissolution of metals. *Analytical Chemistry*, 31(1):33–39, 1959. ISSN 0003-2700.

[52] H. Matsuda and Y. Ayabe. Polarographische untersuchungen über die kinetik der entladung von komplex-metallionen, insbesondere von hydroxo-und ammin-komplexen des zinks. *Ber. Bunsenges. phys. Chem.*, 63(9-10):1164–1171, 1959. ISSN 0005-9021.

[53] J. O'M. Bockris, Z. Nagy, and A. Damjanovic. On the deposition and dissolution of zinc in alkaline solutions. *J. electrochem. soc.*, 119(3):285–295, 1972. ISSN 0013-4651.

[54] J. Hendrikx, A. van der Putten, W. Visscher, and E. Barendrecht. The electrodeposition and dissolution of zinc and amalgamated zinc in alkaline solutions. *Electrochim. Acta*, 29(1):81–89, 1984. ISSN 0013-4686.

[55] A. Rethinam, G. Ramesh Bapu, and V. Muralidharan. Role of triethanolamine and furfuraldehyde on the electrochemical deposition and dissolution behaviour of zinc. *Indian J. Chem. Technol.*, 11:207 – 212, 2004.

[56] L. Oniciu and L. Mureşan. Some fundamental aspects of levelling and brightening in metal electrodeposition. *J. Appl. Electrochem.*, 21(7):565–574, 1991. ISSN 0021-891X.

[57] L. Chai and J. Klein. Large area, molecularly smooth (0.2 nm rms) gold films for surface forces and other studies. *Langmuir*, 23(14):7777–7783, 2007. ISSN 0743-7463.

[58] I. Reviakine, D. Johannsmann, and R. P. Richter. Hearing what you cannot see and visualizing what you hear: Interpreting quartz crystal microbalance data from solvated interfaces. *Anal. Chem.*, 83(23):8838–8848, 2011. ISSN 0003-2700.

[59] M. P. Seah, I. S. Gilmore, and G. Beamson. Xps: binding energy calibration of electron spectrometers 5-re-evaluation of the reference energies. *Surf. Interface Anal.*, 26(9):642–649, 1998. ISSN 0142-2421.

[60] J. Zuo and A. Erbe. Optical and electronic properties of native zinc oxide films on polycrystalline zn. *Phys. Chem. Chem. Phys.*, 12(37):11467–11476, 2010. ISSN 1463-9084.

[61] D. Nečas and P. Klapetek. Gwyddion: an open-source software for spm data analysis. *Cent. Eur. J. Phys.*, 10(1):181–188, feb 2012. ISSN 1644-3608.

[62] MMS AG Membrane Systems. Membrane solutions for the laboratory, 2020. URL https://mmsx.com/site/assets/files/1570/mms_memtester_brochure_en_2020-1.pdf. Accessed: 2023-10-18.

[63] G. F. Tiétcha, L. E. Mears, D. Dworschak, M. Roth, I. Klüppel, and M. Valtiner. Adsorption and diffusion moderated by polycationic polymers during electrodeposition of zinc. *ACS Applied Materials and Interfaces*, 12(26):29928–29936, 2020. ISSN 1944-8244.

[64] J. W. Diggle and A. Damjanovic. The inhibition of the dendritic electrocrystallization of zinc from doped alkaline zincate solutions. *J. Electrochem. Soc.*, 119(12):1649–1658, 1972. ISSN 0013-4651.

[65] J. Bressan and R. Wiart. Inhibited zinc electrodeposition: electrode kinetics and deposit morphology. *J. Appl. Electrochem.*, 9(1):43–53, 1979. ISSN 0021-891X.

[66] R. A. L. Jones. *Tethered polymer chains in solutions and melts*, pages 244–292. Cambridge University Press, 1999.

References

[67] A.J. Bard and L.R. Faulkner. *Electroactive layers and modified electrodes*, book section 14. Wiley Textbooks, 2nd edition, 2000. ISBN 9781118312803.

[68] C. H. Hamann, A. Hamnett, and W. Vielstich. *Electrical Potentials and Electrical Current*, page 550. Wiley, 2nd edition, 2007. ISBN 978-3-527-31069-2.

[69] J. N. Israelachvili. *Intermolecular and Surface Forces*. Academic Pres, 3 edition, 2011.

[70] C. E. Housecroft and E. C. Constable. *Coordination complexes of the d-block metals*, book section 23. Prentice Hall, 3rd edition, 2005.

[71] L. H. Gade. *Koordinationschemie*. Wiley-VCH Verlag GmbH, 2013. ISBN 9783527295036.

[72] J. A. Rodriguez and J. Hrbek. Metal–metal bonding on surfaces: Zn–au on ru(001). *J. Chem. Phys.*, 97(12):9427–9439, 1992.

[73] R. T. Carvalhal, R. Freire, and L. Kubota. Polycrystalline gold electrodes: A comparative study of pretreatment procedures used for cleaning and thiol self-assembly monolayer formation. *Electroanalysis*, 17:1251–1259, 2005.

[74] M. Doi and S. F. Edwards. *The Zimm model*, book section 4.2. Clarendon Press, 1988. ISBN 9780198520337.

[75] G. F. Tiétcha, I. Klüppel, M. Kogler, M. Valtiner, and L. L. E. Mears. Visualizing electrochemical zinc deposition and the role of a polymer additive in the crystal growth mechanism. *Materials and Corrosion*, n/a(n/a):1–10, 2023. ISSN 0947-5117.

[76] E. Kester, U. Rabe, L. Presmanes, Ph. Tailhades, and W. Arnold. Measurement of young's modulus of nanocrystalline ferrites with spinel structures by atomic force acoustic microscopy. *Journal of Physics and Chemistry of Solids*, 61(8):1275–1284, 2000. ISSN 0022-3697.

[77] Q. Guo, L. Zhang, A.S. Zeiger, Y. Li, K. J. Van Vliet, and C. V. Thompson. Compositional dependence of young's moduli for amorphous cu–zr films measured using combinatorial deposition on microscale cantilever arrays. *Scripta Materialia*, 64(1): 41–44, 2011. ISSN 1359-6462.

[78] J.J. Roa, G. Oncins, F.T. Dias, V.N. Vieira, J. Schaf, and M. Segarra. Afm as an alternative for young's modulus determination in ceramic materials in elastic deformation regime. *Physica C: Superconductivity*, 471(17):544–548, 2011. ISSN 0921-4534.

[79] S.-Y. Lang, Y. Shi, X.-C. Hu, H.-J. Yan, R. Wen, and L.-J. Wan. Recent progress in the application of in situ atomic force microscopy for rechargeable batteries. *Current Opinion in Electrochemistry*, 17: 134–142, 2019. ISSN 2451-9103. Environmental Electrochemistry • Surface Electrochemistry.

[80] T. Thomé, S. Fouchez, and S. Delalande. Determination of silicone coating young's modulus using atomic force microscopy. *Physica B: Condensed Matter*, 404(1):22–25, 2009. ISSN 0921-4526.

[81] A. Kalinin, V. Atepalikhin, O. Pakhomov, A. L. Kholkin, and A. Tselev. An atomic force microscopy mode for nondestructive electromechanical studies and its application to diphenylalanine peptide nanotubes. *Ultramicroscopy*, 185:49–54, 2018. ISSN 0304-3991.

[82] M. V. Maslova, L. G. Gerasimova, and W. Forsling. Surface properties of cleaved mica. *Colloid Journal*, 66(3):322, 2003.

[83] A. Christiansen and B. Ridge. Hair and fabric conditioning compositions containing polymeric ionenes. US Patent 4157388, 06 1979.

[84] T. Voss, J. Schulze, A. Kirbs, A. Soenmez, H. Brunner, B. Froese, and U. Engelhardt. Electroplating additive for the deposition of metal, a binary, ternary, quaternary or pentanary alloy of elements of group 11 (ib)-group 13 (iiia)-group 16 (via). US Patent 2011/0094583 A1, 04 2011.

[85] H. Brunner, L. Kohlmann, A. Witczak, and O. Mann. Imidazoyl urea polymers and their use in metal or metal alloy plating bath compositions. EP Patent 3 135 709 A1, 03 2017.

[86] W. E. Eckles. Polyamine brightening agent. US Patent 2013/0175179 A1, 07 2013.

[87] Y. Zhengqin, Y. Zhongbin, H. Lei, B. Yun, L. Lili, Z. Jie, Q. Chentun, and C. Gang. Preparation and application of a new

crosslinked polyammonium as a shale inhibitor. *Journal of Applied Biomaterials and Functional Materials*, 16:119–124, 2018.

[88] L. Xing, J.-R. Liu, X. Hong, K. N. Houk, and C. K. Luscombe. An exception to the carothers equation caused by the accelerated chain extension in a pd/ag cocatalyzed cross dehydrogenative coupling polymerization. *Journal of the American Chemical Society*, 144(5):2311–2322, 2022.

[89] W. H. Carothers. Polymers and polyfunctionality. *Trans. Faraday Soc.*, 32:39–49, 1936.

[90] C. Andrle and T.W. Jelinek. *Hull-Zelle zur Untersuchung von galvanischen Elektrolyten*. Eugen G. LEUZE Verlag, 1 edition, 2007. ISBN 3-87480-224-8.

[91] W. Giurlani, E. Berretti, and A. Lavacchi. Coating thickness determination using x-ray fluorescence spectroscopy: Monte carlo simulations as an alternative to the use of standards. *Coatings*, 9: 79, 01 2019.

[92] W. Giurlani, E. Berretti, M. Innocenti, and A. Lavacchi. Measuring the thickness of metal films: A selection guide to the most suitable technique. *Materials Proceedings*, 2(1), 2020. ISSN 2673-4605.

[93] W. Giurlani, E. Berretti, and A. Lavacchi. Measuring the thickness of metal coatings: A review of the methods. *Coatings*, 10, 12 2020.

[94] D. Beamish. Coating thickness measurement. *Metal Finishing*, 108(11):379–385, 2010. ISSN 0026-0576.

[95] N. Erdman, R. Campbell, and S. Asahina. Artifact-free cross-sections. *Advanced Materials and Processes*, 164:33–35, 07 2006.

[96] F. Haider, S. Suryanto, M. H. Ani, and M. Mahmood. A comparison between destructive and non-destructive techniques in determining coating thickness. *IOP Conference Series: Materials Science and Engineering*, 290:1–6, 01 2018.

[97] M. Goslinska, I. Selmer, C. Kleemann, U. Kulozik, I. Smirnova, and S. Heinrich. Novel technique for measurement of coating

layer thickness of fine and porous particles using focused ion beam. *Particuology*, 42:190–198, 06 2018.

[98] V. Rupetsov and R. Minchev. Experimental calo tester for the coating thickness measurement, 06 2016.

[99] K.-N. Joo. Method and apparatus for performing film thickness measurements using white light scanning interferometry. EP Patent 2 482 031 A1, 08 2012.

[100] P. Picart, M. Malek, and J. Garcia-Sucer-Quia. Method for determining the thickness of thin layer by multi-wavelength interferometry and corresponding computer program package, storage means and system. WO Patent 2016/091983A1, 06 2016.

[101] W. Demtröder. *Experimentalphysik 2: Elektrizität und Optik*. Springer Berlin Heidelberg, 7 edition, 2018. ISBN 9783662557891.

[102] P. Hariharan. Chapter 1 interferometry: Its development. In *Optical Interferometry (Second Edition)*, pages 1–8. Academic Press, San Diego, second edition edition, 2003. ISBN 978-0-12-311630-7.

[103] attocube systems AG. Ids3010 work principle, 2019. URL https://www.attocube.com/en/ressources/webinars-scientific-presentations-videos/videos. Accessed: 2023-05-06.